Immobilized FhuD2 Siderophore-Binding Protein Enables Purification of Salmycin Sideromycins from *Streptomyces violaceus* DSM 8286

Gerry Sann M. Rivera, Catherine R. Beamish, and Timothy A. Wencewicz*

Department of Chemistry, Washington University in St. Louis, One Brookings Drive, St. Louis, MO 63130, United States

*Correspondence to TAW: Email: wencewicz@wustl.edu; Ph: 314-935-7247; Fax: 314-935-4481; ORCID: 0000-0002-5839-6672

Siderophores are a structurally diverse class of natural products common to most bacteria and fungi as iron(III)-chelating ligands. Siderophores, including trihydroxamate ferrioxamines, are used clinically to treat iron overload diseases and show promising activity against many other iron-related human diseases. Here we present a new method for the isolation of ferrioxamine siderophores from complex mixtures using affinity chromatography based on resin-immobilized FhuD2, a siderophore-binding protein (SBP) from *Staphylococcus aureus*. The SBP-resin enabled purification of charge positive, charge negative, and neutral ferrioxamine siderophores. Treatment of culture supernatants from *Streptomyces violaceus* DSM 8286 with SBP-resin provided an analytically pure sample of the salmycins, a mixture of structurally complex glycosylated sideromycins (siderophore-antibiotic conjugates) with potent antibacterial activity towards human pathogenic *Staphylococcus aureus* (MIC = 7 nM). Siderophore affinity chromatography could enable the rapid discovery of new siderophore and sideromycin natural products from complex mixtures to aid drug discovery and metabolite identification efforts in a broad range of therapeutic areas.

Keywords

desferrioxamine B, affinity chromatography, siderophore-antibiotic conjugate, drug delivery, metal chelation therapy, iron transport

Natural products continue to be a major source of lead molecules for drug discovery efforts in many therapeutic areas.[1, 2] Siderophores are iron(III)-chelating natural products biosynthesized and excreted by bacteria and fungi to aid in iron acquisition.[3, 4] Siderophores typically have high-affinity and selectivity for iron(III) imparted by oxygen-rich chelating groups such as catecholates, hydroxamates, and α-hydroxycarboxylates.[5] Siderophores have been investigated in clinical applications for metal chelation therapies aimed at treating iron overload diseases.[6] Desferal®, also know as desferrioxamine B, is a naturally occurring linear trihydroxamate siderophore from *Streptomyces pilosus* that is FDA-approved for the treatment of human iron overload diseases, including β-thalassemia (**Figure 1**).[7] Ferrioxamine siderophores have also been explored as treatments for neurological disorders such as Parkinson's disease,[7] chronic pulmonary disease (COPD),[8] wound healing,[9] malaria,[10] and cancer.[11]

Natural functions of microbial siderophores include metal transport, toxic metal sequestration, quorum sensing, protection from oxidative stress, virulence, and chemical defense.[12] The biosynthesis of bacterial siderophores is under transcriptional control of ferric uptake regulator (FUR) proteins.[13] Under iron-restrictive conditions, siderophore biosynthesis[14] takes place in the cytoplasm followed by efflux of the mature siderophore scaffold to the extracellular space.[15] Siderophores bind iron(III) with extraordinary affinity (stability constants can be as high as 10^{42}) and can solubilize and/or strip the metal directly from environmental and biological sources (e.g. transferrin).[4, 5] In Gram-negative bacteria, high-affinity outer membrane-imbedded receptor proteins (OMRs) bind the soluble siderophore-iron(III) complex and facilitate import with assistance from the TonB-ExbB-ExbD protein complex and a proton-motive force.[16] Soluble periplasmic siderophore-binding proteins (SBPs) ferry the siderophore-iron(III) complex to ATP-dependent ABC-type transporters that couple ATP-hydrolysis to cytoplasmic transport.[17-20] Enzymatic reduction of iron(III) to iron(II) secures the intracellular iron[21, 22] and provides recycled *apo*-siderophore.[23-26] Alternatively, reductive iron release can take place in the periplasm of Gram-negative bacteria.[27] In some cases, enzymatic degradation of the siderophore scaffold is necessary to retrieve iron from the stable siderophore chelate.[28] Analogous siderophore utilization pathways are operative in Gram-positive bacteria with the exception of OMRs

and the TonB-ExbB-ExbD protein complex.[29] Instead, SBPs are displayed on the cell surface as membrane-anchored lipoproteins that directly sequester extracellular siderophore-iron(III) complexes and interface with ATP-hydrolyzing ABC-transporters to drive import. Some OMRs and SBPs are expressed to enable the utilization of siderophores produced by neighboring organisms, so called xenosiderophores,[30] which provide a competitive growth advantage.[31] Xenosiderophore utilization can be countered by the production of sideromycins,[32] siderophore-antibiotic conjugates (SACs), which deliver a potentially toxic antibiotic upon internalization.[33] Natural sideromycins and synthetic SACs represent an attractive approach for pathogen-targeted antibiotic delivery and have served as tools and inspiration for the study of siderophore pathways in bacteria and fungi.[32, 34]

More than 500 naturally occurring siderophore structures have been reported in the literature.[4] The ferrioxamine family of siderophores is common to many soil-dwelling Streptomyces and marine bacteria.[30, 35-37] Ferrioxamine siderophores are composed of repeating units of *N*-hydroxy-putrescine and/or cadaverine joined by succinyl groups that provide the carbonyl for the metal chelating hydroxamate ligand.[7, 38] Three sequential hydroxamate ligands in the ferrioxamine backbone provides an ideal template for chelating iron(III) with octahedral geometry, 1:1 siderophore:iron(III) stoichiometry, and stability constants (K_{Fe}) on the order of 10^{30}.[4] Ferrioxamine biosynthesis is driven by the conserved operon *desABCD*,[39] which has enabled chemoenzymatic synthesis and virtual mining for new ferrioxamine siderophores.[39-43] However, many siderophore biosynthetic gene clusters (BGCs) remain silent under standard culture conditions and many siderophore-producing microbes are difficult to grow in the laboratory using standard cultivation techniques.[44, 45] The discovery of new natural products, including siderophores, is further limited by laborious scale-up and purification from microbial cultures.[3, 4] Historically, siderophore production and purification has been guided by the extraordinary affinity for iron(III). The chrome azurol s (CAS) assay is a colorimetric test for siderophore production that can be applied to culture supernatants or directly incorporated into bacterial growth media.[46, 47] Technological advances in high-resolution mass spectrometry,[48] comparative metabolomics,[49] microbial cultivation,[44, 50] synthetic biology,[51] comparative transcriptomics,[52] metagenomics,[53, 54] microbial genome-mining,[55] and high-throughput

screening[56] have enabled the discovery of new natural products,[57] including siderophores.[58-60] Recently, a new structural class of siderophores, the crochelins, was discovered in *Azotobacter chrococcum* culture supernatants using the "chelome" metabolomics platform that searches high-resolution LC-MS/MS data for the mass isotopes of iron.[48, 61] Similarly, the siderophore nicoyamycin A was isolated from a library of 32,879 natural product extracts using a screen for growth inhibition of uropathogenic *E. coli* (UPEC) under low iron conditions.[62] In both cases, preparative purification of the metal-chelating siderophores from microbial fermentations required challenging chromatographic steps.

Natural product isolation and purification is challenging no matter how the metabolite is discovered. Efforts to improve the purification of natural products from complex mixtures include advancements in fermentation, strain prioritization, heterologous expression, bioengineering, chromatography, and fractionation.[63] The unique structural complexity of natural products can be leveraged for various types of affinity chromatographies.[64] Chemoselective enrichment chromatography has been used to covalently capture target natural product classes from complex extracts.[65] Methods for the chemoselective enrichment of natural products containing hydroxyl,[66] polyol,[67] carboxylate,[68] amine,[69] thiol,[70] ketone/aldehyde,[71] and conjugated diene[72-74] functional groups have been reported. However, chemoselective functionalization of complex natural product scaffolds is a prerequisite for covalent capture on an immobilization resin and this remains a challenge in synthetic organic chemistry.[75] Furthermore, natural product functionalization must be reversible in order to release the immobilized metabolite and obtain the native structure for accurate characterization.[76] Metal chelation has been exploited as a reversible, chemoselective method to purify metal-chelating natural products, including siderophores.[37, 77] Nickel(II)-based immobilized affinity chromatography (IMAC) has been used to purify hydroxamate-containing desferrioxamine siderophores from microbial cultures,[77] in a similar manner as conventional purification of polyhistidine-tagged proteins. Boronate affinity chromatography has also been used to purify catechol-based siderophores.[78] Both boronate and Ni-IMAC methods are selective for metal-free

siderophores, which can be problematic for siderophores that readily form high-affinity and thermodynamically stable metal chelates.[4]

Protein-ligand affinity chromatography is a highly specific purification method that can exploit the strong binding affinity of a natural product for its biological target.[79, 80] Affinity chromatography has been applied in both targeted[81] and untargeted[82] approaches to isolate numerous natural product classes. Affinity selection-mass spectrometry (ASMS) has emerged as a promising method for small molecule drug discovery.[83] ASMS utilizes an immobilized target that is exposed to a library of compounds followed by elution with known ligands. Alternatively, immobilized or tagged natural products, including siderophores, can be utilized for protein pull-down assays to reveal biological targets from cell lysates.[84, 85] For example, a biotinylated version of the siderophore petrobactin was immobilized to avidin resin to enable the direct identification of the petrobactin import protein in pathogenic *Bacillus anthracis*.[86] Siderophores have also been immobilized on surfaces for applications in metal sequestration,[87] surface adhesion,[88] and pathogen detection.[89-92] For these types of applications, covalent modification of the siderophore is often required and carries the risk of perturbing the affinity for target proteins. However, the reversibility, stoichiometric binding, and low dissociation constants (typically nanomolar[31]) makes the siderophore-SBP interaction attractive for affinity applications. Immobilization of SBPs using standard protein-resin immobilization techniques presents the opportunity for sequestration of natural, unmodified siderophore metabolites. To the best of our knowledge, immobilized SBPs have never been used to sequester siderophores from complex mixtures (at least intentionally since heterologous expression and affinity purification of some SBPs can result in co-purification with a siderophore ligand).[93, 94] However, in one report soluble CntA, an SBP from *S. aureus*, was incubated with *S. aureus* culture supernatant to sequester a Ni-bound metabolite later identified as the metallophore staphylopine, which is an important *S. aureus* virulence factor.[95, 96]

Here, we sought to streamline the isolation of siderophores from complex mixtures by leveraging the high specificity and affinity of SBPs for siderophore ligands (**Figure 2**). We developed a versatile affinity chromatography platform for sequestering ferrioxamine

siderophores by adhering an *N*-His_6-tagged SBP (FhuD2 from *S. aureus*) to Ni(II)-charged nitriloacetic acid agarose (Ni-NTA) resin. We used the SBP-resin to purify charge positive, charge negative, and charge neutral ferrioxamine siderophores. The SBP-resin is stable and can be cycled repetitively by loading siderophores of interest and displacing with sacrificial siderophores that are easily separated based on net charge using ion exchange chromatography. We used the FhuD2 SBP-resin to isolate the salmycins, a mixture of glycosylated sideromycins, from fermentation extracts of *Streptomyces violaceus* DSM 8286. The use of affinity chromatography greatly simplifies the purification of the salmycins and rapidly provides analytically pure material suitable for quantitative biological assays. Our SBP-resin could be interfaced with existing natural product discovery platforms to selectively survey for ferrioxamine siderophores in diverse environments.

Results & Discussion

Designing a siderophore-binding resin.

Bacteria rely on two types of siderophore receptors as gatekeepers for cell entry, OMRs from the transmembrane beta-barrel superfamily and soluble SBPs from the type III class of the substrate-binding protein superfamily.[97] OMRs present challenges for *in vitro* study due to lack of solubility using standard heterologous protein expression.[16] SBPs are well known for having high aqueous solubility and stability. SBPs from Gram-negative bacteria are expressed with an *N*-terminal signal sequence that directs secretion to the periplasm with signal peptidase-mediated cleavage of the signal peptide. Periplasmic SBPs are highly soluble and efficiently expressed using heterologous methods.[17, 31] SBPs from Gram-positive bacteria are co-expressed with an *N*-terminal signal sequence that is cleaved during secretion. SBPs are displayed as covalently anchored lipoproteins on the surface of Gram-positive bacteria.[29] Typically, SBPs are selective for binding a general structural class of siderophores (e.g. ferrioxamines), but broadly bind structural analogs within the class. The high solubility and broad substrate-binding ability of SBPs make these proteins excellent candidates for heterologous expression and *in vitro* study.[31]

We identified FhuD2 as a promising SBP for siderophore-affinity chromatography. FhuD2 is selective for binding trihydroxamate siderophores, including the ferrioxamines, in both the iron-free and iron-bound forms.[31] Pathogenic strains of *S. aureus*, including methicillin-resistant *S. aureus* (MRSA), display the SBP FhuD2 on the cell surface as a virulence factor during infection.[98] The hydrophobic, charge-neutral siderophore-binding site in FhuD2 accomodates a wide range of ferrioxamine siderophores including charge positive, charge negative, neutral, and sterically bulky analogs.[99] Truncated FhuD2 lacking the lipopeptide signal sequence is soluble and maintains the ability to bind ferrioxamine siderophores and sideromycins carrying large antibiotic cargos with nanomolar affinity.[31] We envisioned a simple strategy for using immobilized FhuD2 to sequester ferrioxamine siderophores in analogy to established methods for performing affinity chromatography (**Figure 2a**). We hypothesized that adhering the soluble domain of FhuD2 to Ni-NTA resin via a hexahistidine linker would provide an SBP-resin selective for binding ferrioxamine siderophores. The SBP-resin could be treated with a solution of the siderophore of interest (S_1) to load S_1 in the FhuD2 binding pocket. After washing with buffer, S_1 could be eluted by treating the SBP-resin with a solution of a sacrificial siderophore (S_2) that can displace S_1 from the FhuD2 binding site. Excess S_2 could be removed from S_1 using simple ion exchange chromatography if the net charge of the two siderophores is different. In theory, any SBP could be immobilized for biased and unbiased siderophore sequestration (**Figure 2b**). We selected FhuD2 to enable unbiased isolation of hydroxamate-based siderophores because of its known siderophore promiscuity. Other SBPs are highly selective and might enable biased, targeted isolation of siderophores.[29] Genes encoding for SBPs are often clustered in operons with siderophore biosynthesis genes.[14] Heterologous expression and immobilization of SBPs from siderophore BGCs might enable biased isolation of the cognate siderophore from cultures of the producing microbe.

Functional validation of SBP-resin.

We used heterologous expression in *E. coli* BL21(DE3) to overproduce a truncated version of FhuD2, FhuD2Δ24, replacing the first 24 amino acids with a *N*-terminal hexahistidine motif to facilitate purification using Ni-NTA resin (**Supplementary Table 2**).[31] Protein

purity was assessed to be >95% by ESI-MS and SDS-PAGE analysis (**Supplementary Fig. 1,2**). ESI-MS analysis of purified *N*-His_6-FhuD2Δ24 showed an intact hexahistidine motif and loss of the *N*-terminal methionine residue. *N*-His_6-FhuD2Δ24 is highly soluble in aqueous buffer and is stable towards repeated freeze-thawing. After dialysis of the purified protein into phosphate buffer, we loaded fresh Ni-NTA resin to capacity with *N*-His_6-FhuD2Δ24 forming the SBP-resin (~0.2 μmol FhuD2Δ24/mL; resin loaded to capacity was judged by SDS-PAGE analysis of column flowthrough). We chose the model siderophores ferrioxamine (**FO**), succinylferrioxamine (**SFO**), and acetylferrioxamine (**AcFO**) as iron(III) complexes to validate capacity of the FhuD2 SBP-resin to reversibly bind trihydroxamate siderophores (**Figure 1**). FhuD2Δ24 is proposed to catalyze the exchange of iron(III) between ferrioxamine siderophores.[100, 101] Desferrioxamine (**DFO**) has been shown to form coordination complexes with Ni-NTA resin.[77, 102] To avoid complications from iron exchange and non-specific chelation to the Ni-NTA resin, we used the iron(III)-bound forms of the siderophores. **FO** (net +1 charge), **SFO** (net -1 charge), and **AcFO** (neutral) were chosen based on differences in polarity and net charge in order to facilitate ion exchange separation of target siderophore (S_1) and sacrificial siderophore (S_2) from the SBP-resin column elution. Passing **FO**, **SFO**, and **AcFO** through Ni-NTA resin without immobilized FhuD2Δ24 resulted in no detectable, non-specific adherence to the resin. We used an intrinsic fluorescence-quenching assay to confirm that our recombinant *N*-His_6-FhuD2Δ24 protein binds **FO**, **SFO**, and **AcFO** with the anticipated nanomolar affinity (**Supplementary Fig. 4**).[31] FhuD2Δ24 tryptophan fluorescence is strongly quenched upon ferrioxamine siderophore binding, presumably due in part to W197, which directly contacts the ferrioxamine backbone through a stabilizing hydrogen bond.[99] Apparent K_d values of *N*-His_6-FhuD2 for **FO**, **SFO**, and **AcFO** were 53 ± 6 nM, 46 ± 7 nM, and 31 ± 4 nM, respectively, indicating that all three siderophores form 1:1 stoichiometric complexes with soluble *N*-His_6-FhuD2Δ24.

In order for the SBP-resin to function as an affinity chromatography platform, the resin must bind to a target siderophore S_1 and subsequently release S_1 in the presence of a sacrificial siderophore S_2 that is added in excess. Presumably, excess S_2 can competitively displace S_1 from the SBP-resin resulting in S_2-saturated resin and an elution containing a

mixture of S_1 and S_2 (**Figure 2a**). We validated this approach using all six possible combinations of **FO**, **SFO**, and **AcFO** as S_1 and S_2 and confirmed elution of S_1 from the SBP-resin using LC-MS (**Figure 3a**). Siderophore S_1 was loaded at 0.1 mg/mL and, after sufficient column washing, was eluted with an equal volume of siderophore S_2 at 0.1 mg/L. When **FO** was used as S_1 the SBP-resin was saturated with **FO** and excess **FO** was detected in the column flowthrough (**Fig. 3b**; blue trace). No **FO** was detected in the column wash (**Fig. 3b**; red trace). Addition of **SFO** as S_2 eluted **FO** from the SBP-resin (**Fig. 3b**; green trace). The same batch of SBP-resin was immediately used for another cycle of siderophore purification with bound **SFO** now serving as S_1. Excess **SFO** was detected in the column flowthrough suggesting full saturation of the SBP-resin (**Fig. 3c**; blue trace). No **SFO** was detected in the column wash (**Fig. 3c**; red trace). Addition of **FO** as S_2 eluted **SFO** from the SBP-resin (**Fig. 3c**; green trace). Subsequent cycles with remaining S_1:S_2 siderophore pairs were performed in analogous fashion (**FO**:**AcFO**, **Fig. 3d**; **AcFO**:**SFO**, **Fig. 3e**; **SFO**:**AcFO**, **Fig. 3f**; **AcFO**: **FO**, **Fig. 3g**).

These proof-of-principle experiments show that SBP-resin can be cycled with different S_1 and S_2 siderophore combinations for sustained siderophore purification without the need to use fresh resin. The FhuD2Δ24 SBP-resin is robust and does not appear to lose efficiency during repeated use. All combinations of **FO**, **SFO**, and **AcFO** as S_1 and S_2 siderophores provided the desired S_1 siderophore upon elution from the SBP-resin with S_2. The broad scope of the SBP-resin is consistent with the observation that FhuD2 enables broad utilization of trihydroxamate siderophores for iron acquisition in *S. aureus*.[31] Similar FhuD2 K_d values for **FO**, **SFO**, and **AcFO** suggest that the siderophores competitively bind FhuD2 regardless of net siderophore charge (**Supplementary Fig. 4**). To demonstrate this competitive binding, we treated an equimolar mixture of **FO**, **SFO**, and **AcFO** with FhuD2 SBP-resin followed by elution with a fourth ferrioxamine siderophore, danoxamine (**Dan**) (**Supplementary Table 4**). This resulted in competitive binding and elution of all three siderophores with only modest changes in ion counts from load to elution (**Supplementary Fig. 5**; **Supplementary Table 5**). The siderophore-binding pocket of FhuD2 is mostly hydrophobic and charge neutral, which supports the capacity for

accommodating ferrioxamine siderophores with different polarity and electrostatic properties.[99]

Separation of S_1 and S_2 by ion exchange chromatography.

One remaining challenge for using SBP-resin to purify siderophores is that column elutions contain a mixture of the desired siderophore S_1 and the sacrificial siderophore S_2. In our case, both S_1 and S_2 are from the ferrioxamine family and give similar retention times on RP-C18 HPLC. We were able to separate mixtures of siderophores by preparative HPLC, but the large excess of the S_2 siderophore limited injection volume size and decreased peak resolution. We selected **FO**, **SFO**, and **AcFO** for these proof-of-principle studies because of differences in net charge (charge positive, charge negative, and neutral, respectively) that we predicted would enable final separation of S_1 and S_2 siderophores via ion exchange chromatography, which can be performed on FPLC or HPLC platforms.

The eluent from the SBP-resin requires desalting prior to ion exchange chromatography. This can be accomplished using C18 chromatography or by lyophilizing the sample and redissolving siderophores from the bulk solid using methanol. We used a diethylamine cation exchange resin (DEAE) and a Cellex P anion exchange resin to separate various combinations of cationic (**FO**), anionic (**SFO**), and neutral (**AcFO**) siderophores (**Fig. 4a**). Presumably other commercially available cation and anion exchange solid phases would also be suitable for this type of separation. An aqueous solution containing a mixture of **FO** and **SFO** was loaded onto a DEAE resin (**Fig. 4b,c**; blue traces). The column was washed with water to provide cationic **FO** that does not adhere to the cationic DEAE resin (**Fig. 4b,c**; red traces). **SFO** is left bound to the DEAE resin and can be eluted by addition of 4% ammonium hydroxide solution (**Fig. 4b,c**; green traces). Mixtures of **AcFO** and **FO** (**Fig. 4d,c**; blue traces) were treated with Cellex P resin to bind cationic **FO** and provide charge neutral **AcFO** in the column wash (**Fig. 4d,c**; red traces). **FO** was eluted by the addition of 4% ammonium hydroxide solution (**Fig. 4d,c**; green traces). Lastly, mixtures of **AcFO** and **SFO** were separated using DEAE cation exchange resin (**Fig. 4f,g**; blue trace). Anionic **SFO** adhered to the DEAE resin while **AcFO** eluted in the column washes (**Fig. 4f,g**; red traces). **SFO** was eluted by addition of 4% ammonium hydroxide in a manner similar to that

described for the **SFO/FO** mixture (**Fig. 4f,g**; green traces). The use of ion exchange chromatography can expedite the final separation of S_1 and S_2 siderophores obtained from SBP-resin elutions. **FO**, **SFO**, and **AcFO** represent three distinct charge states for siderophores (mono-cationic, mono-anionic, and neutral, respectively) that can be used as the S_2 elution siderophore in applications of the FhuD2Δ24 SBP-resin in the purification of ferrioxamine siderophores from complex environmental samples and microbial fermentations.

Purification of salmycins A–D from S. violaceus DSM 8286.

To demonstrate the utility of the FhuD2Δ24 SBP-resin we sought to purify a natural siderophore from a microbial culture (**Supplementary Fig. 6**). We chose a challenging and structurally complex class of sideromycins, the salmycins, which contain a ferrioxamine siderophore component that is recognized by FhuD2.[103, 104] The salmycins are a mixture of glycosylated sideromycins (**Sal A–D**) produced by *Streptomyces violaceus* DSM 8286.[105] The siderophore portion of **Sal A–D** is a trihydroxamate siderophore from the ferrioxamine family known as danoxamine (**Dan**).[106, 107] Danoxamine is composed of two *N*-hydroxy-cadaverine subunits and a terminal *N*-hydroxy-5-aminopentan-1-ol, or alternatively a terminal *N*-hydroxy-4-aminobutan-1-ol, joined via succinoyl linker groups. In **Sal A–D** the aminodisaccharide antibiotic is covalently linked to danoxamine through a succinoyl ester bond that is likely to be hydrolyzed upon internalization.[108] The potency of the salmycins (minimum inhibitory concentration of ~10 nM in liquid media against planktonic *S. aureus*) is thought to arise from high intracellular concentrations driven by active transport through FhuBCDG.[29, 32, 109-111] Mutations in the *fhuD2* gene confer resistance to the salmycins in *S. aureus* consistent with FhuD2 selecting for cell entry.[32, 104, 108] These findings make our FhuD2Δ24 SBP-resin a promising method for purification of the salmycins from *S. violaceus* cultures.

The salmycins were originally isolated in 1995 from the culture supernatant of *S. violaceus* DSM 8286.[103] In the original report by Vértesy and coworkers and two subsequent patents from the same group a series of hydrophobic resins, ion exchange columns, and RP-C18

chromatgraphy steps provided analytically pure salmycins suitable for full characterization.[112, 113] A large scale up (185 L of culture) was used to provide milligram quantities of **Sal A–D** and enabled the separation of isomers. In our hands, and others,[104] reproducing this purification scheme has failed to provide analytically pure samples of the salmycins. During our purification attempts from 12 x 1 L batch cultures of *S. violaceus* DSM 8286 following patent protocol we identified an unknown contaminant with retention time and *m/z* values by LC-MS that co-elute with the salmycins (**Supplementary Fig. 12**). As a result, LC-MS analysis of *S. violaceus* DSM 8286 culture supernatants and solutions from various purification steps was challenging and we were never able to obtain a salmycin sample free of the unknown impurity, even after multiple rounds of preparative HPLC chromatography using RP-C18 and HILIC columns. The unknown impurity lacks antibacterial activity, so bioactivity guided fractionation was informative during purification of the salmycins. Agar diffusion antibacterial susceptibility assays using salmycin-sensitive *S. aureus* ATCC 11632 provided a sensitive assay for the presence of salmycins when coupled to a sister medium containing **FO**, which antagonizes the growth inhibitory activity of the salmycins by competing for FhuD2-mediated uptake.[33, 108] We aimed to use FhuD2Δ24 SBP-resin and bioactivity guided fractionation to purify the salmycins directly from *S. violaceus* DSM 8286 cultures to overcome co-elution of the impurities during traditional chromatographic steps.

We started with 10 L of *S. violaceus* DSM 8286 culture supernatant that was filtered through celite, concentrated, and washed with MeOH. Bioactivity assays suggested that the MeOH washings contained the salmycins. The MeOH washings were concentrated and dissolved in pure H_2O in preparation for treatment with SBP-resin. LC-MS analysis of the column loading solution showed a strong signal in the Exctracted Ion Chromatogram (EIC) for the *m/z* value (1053) corresponding o the $[M+H]^+$ ion of the **Sal A** iron(III) complex (**Fig. 5**; blue trace, retention time = 4.9 min). Mass signatures for other salmycin isomers were also observable by LC-MS (**Supplementary Fig. 10**). Unknown impurities with broad peak patterns were also present in the *m/z* 1053 EIC of the load sample. When tested against *S. aureus* ATCC 11632 on solid media the load solution gave a strong zone of growth inhibition. The flowthrough from the SBP-resin showed decreased ion counts for *m/z* 1053

peak corresponding to **Sal A**, but still contained the broad unknown impurity peaks (**Fig. 5**; red trace) that was accompanied by a decrease in the size of the growth inhibition zone when tested against *S. aureus* ATCC 11632. Buffer washes of the SBP-resin gave no detectable ion counts for *m/z* 1053 corresponding to **Sal A** in the EIC (**Fig. 5**; green trace) and showed no growth inhibition against *S. aureus* ATCC 11632. After elution of the SBP-resin with a dilute solution of **Dan** the ion counts for *m/z* 1053 in the EIC returned (**Fig. 5**; magenta trace) along with a noticeable zone of growth inhibition when tested against *S. aureus* ATCC 11632. The zone of growth inhibition for the elution was hazy due to the **excess Dan** in the sample, which antagonizes salmycin transport in *S. aureus*. Further purification by RP-C18 preparative HPLC (**Supplementary Fig. 8**) provided a pure sample of the salmycins free of **Dan** with potent antibacterial activity (**Fig. 5**; olive trace). Purification of the salmycins by FhuD2Δ24 SBP-resin proceeded smoothly in a similar manner observed for combinations of **FO**, **SFO**, and **AcFO** used in the proof-of-principle studies. **Dan** was used as the eluting siderophore S_2 instead of **FO** to increase separation of retention times on RP-C18 HPLC (**Supplementary Fig. 8**). The SBP-resin was tolerant of the complex media and could be recycled as done for the model siderophores. The amount of salmycin that can be purified from *S. violaceus* DSM 8286 is limited by the amount of FhuD2 employed due to 1:1 stoichiometric binding of salmycin by FhuD2.[99] Thus, scaling up the purification will require scaling up FhuD2 production. Fortunately, FhuD2 expresses at high levels in our *E. coli* BL21 expression system and is highly soluble, stable, and tolerant of handling/immobilization.[31] Industrial scale precedent with maltose-binding protein (MBP),[114, 115] a substrate-binding protein that is structurally related to FhuD2, suggests that this type of scale-up is achievable. FhuD2Δ24 SBP-resin does not separate individual salmycin isomers, but enrichment using SBP-resin enhances HPLC peak resolution that might aid in final chromatographic separation of individual isomers (**Supplementary Fig. 9**).

We also explored the treatment of *S. violaceus* DSM 8286 culture supernatant with HP20 and DEAE resins prior to siderophore-affinity chromatography (**Supplementary Fig. 7**). We found that this treatment was not necessary when using FhuD2Δ24 SBP-resin, but was required for the use of centrifugal filtration since the culture supernatant frequently

clogged the 30K molecular weight cut-off semi-permeable membranes. We used centrifugal filtration to scale up the salmycin purification and provide enough material for characterization. The molecular formulas of **Sal A–D** were confirmed by high-resolution LC-mass spectrometry (**Supplementary Fig. 10,11**). We also measured the optical absorbance properties, FhuD2 K_d binding constant, iron(III) binding affinity (K_{Fe}), and MIC value towards *S. aureus* ATCC 11632 (**Supplementary Fig. 13**). The UV-Vis absorbance spectrum was consistent with other trihydroxamate siderophores bound to iron(III) with a characteristic peak at 427 nm arising from ligand-to-metal interactions (**Supplementary Fig. 13a**). Assuming an extinction coefficient of 3000 $M^{-1}cm^{-1}$ (common for most 1:1 ferrioxamine:iron(III) complexes),[31] we quantified stock solutions of the salmycins to measure FhuD2Δ24 K_d, K_{Fe}, and MIC values. The salmycins quenched the intrinsic fluorescence of *N*-His_6-FhuD2Δ24 similar to **FO**, **SFO**, and **AcFO** (**Supplementary Fig. 13b**). Fluorescence quenching of *N*-His_6-FhuD2Δ24 was used to estimate the apparent K_d value of 43 ± 6 nM for the salmycins in close proximity with the apparent K_d values for **FO**, **SFO**, and **AcFO** (53 ± 6 nM, 46 ± 7 nM, and 31 ± 4 nM, respectively). The aminoglycoside moiety does not appear to reduce affinity for FhuD2, which is consistent with binding studies performed with structurally related SACs.[31-33] We used an EDTA competition assay to measure the apparent K_{Fe} for the salmycins (**Supplementary Fig. 13c**). Treatment of iron(III)-bound salmycins with a slight excess of EDTA led to rapid exchange of iron and equilibration as judged by continuous monitoring of optical absorbance at 427 nm. The log K_{Fe} was calculated to be 25.5 ± 0.1, which is similar to the log K_{Fe} reported for a synthetic danoxamine-ciprofloxacin (25.6 ± 0.1) and the parent siderophore **Dan** (27.8 ± 0.3).[31] The log K_{Fe} value of **FO** is 30.3 ± 0.4 with the gain in iron(III) affinity arising from the simple change of a terminal hydroxyl group to a terminal primary amine that is protonated at physiological pH. **FO** is known to promote the growth of *S. aureus* ATCC 11632 more efficiently than **Dan** under iron-limiting conditions.[31] **FO** is also more antagonistic towards a danoxamine-ciprofloxacin SAC in antibacterial susceptibilities assays for *S. aureus*.[33] We showed the same effect for the salmycins using an agar diffusion antibacterial susceptibility assay with *S. aureus* ATCC 11632 (**Supplementary Fig. 13d**). The salmycins alone gave a well-defined zone of growth inhibition against *S. aureus* ATCC 11632. In the presence of a

20-fold excess of **Dan** we observed a small, hazy zone of growth of inhibition. In the presence of a 20-fold excess of **FO** there was no visible zone of growth inhibition and the antibacterial activity of the salmycins was abolished. The salmycins contain a secondary amine as part of the aminoglycoside antibiotic that is predicted to make the salmycin iron(III) complex mono-cationic under physiological conditions. We previously showed that mono-cationic ferrioxamine siderophores, like **FO**, outperform mono-anionic ferrioxamine siderophores, like **Dan**, in *S. aureus* growth promotion assays.[31] Our current findings are consistent with this observation and suggest that mono-cationic salmycins will be competitive with other ferrioxamine siderophores in microenvironments to gain cell entry through ferrioxamine uptake systems. With analytically pure salmycins in hand we also set out to confirm the literature reported MIC value of ~10 nM against strains of *S. aureus*.[32, 104, 108] We used the broth microdilution method in Mueller-Hinton No. 2 broth made iron-deficient by the addition of 2,2-dipyridyl to measure an MIC value of 7.8 nM against *S. aureus* ATCC 11632, confirming the original literature value.

Summary, conclusions, and outlook.

We have developed a new affinity chromatography strategy for purifying siderophores by immobilizing a His-tagged SBP on Ni-NTA resin. We utilized FhuD2 from pathogenic *S. aureus* as the SBP because of its ability to broadly bind trihydroxamate siderophores from the ferrioxamine family. Our FhuD2Δ24 SBP-resin enabled sequestration of mono-cationic (**FO**), mono-anionic (**SFO**), and neutral (**AcFO**) ferrioxamines. Siderophore binding was reversible and all siderophores could be displaced from the SBP-resin using an excess of competing siderophore with similar binding affinity for FhuD2Δ24. To validate the utility of SBP-resin in natural product isolation, we purified the salmycins from *S. violaceus* DSM 8286 culture supernatants to greatly simplify the isolation of these structurally complex sideromycins. There is growing interest in the discovery of new siderophores and sideromycins to treat a variety of human diseases, including infectious diseases.[12, 34, 116] SBP-resin coupled with microbial cultivation, genome mining, metabolomic, transcriptomic, and high-throughput screening might expedite the discovery of new siderophores. SBP-resin might also be useful for purifying synthetic siderophores,

sideromycins, and siderophore conjugates that often require final purification by tedious chromatographic steps.[108] Immobilized SBPs might also be useful for studying siderophore membrane transport paradigms and probing important structure-binding relationships for SBPs and siderophores that might lead to an improved understanding of microbial siderophore utilization.[31, 100, 101] In theory, SBP-resin can be applied as a general affinity-based immobilization strategy for a variety of chemical biology applications in much the same ways as established technologies such as MBP-maltose and avidin-biotin methods,[117] although proof-of-principle studies will be needed to validate this claim.

SBP-resin has several advantages over covalent capture approaches to immobilize siderophores and other natural products.[75] SBP-resin is non-covalent and reversible allowing for mild recovery of immobilized siderophores of interest without structural perturbation through simple displacement with a competing sacrificial siderophore. SBP-resin is highly specific and enables for targeting specific structural classes of siderophores in complex mixtures containing a variety of siderophore types. SBP-resin could be adapted for virtually any siderophore with a soluble, cognate SBP. SBPs are typically selective for specific structural classes of siderophores including hydroxamates, catecholates, and α-hydroxycarboxylates.[4] Presumably some non-specific siderophore binding might take place when trying to sequester target molecules from mixtures containing diverse siderophore structures. Our successful purification of the salmycins from crude *S. violaceus* DSM 8286 cultures using immobilized FhuD2Δ24 suggests that selective siderophore binding can be achieved using a carefully chosen immobilized SBP with the proper structural selectivity. In theory, siderophore BGCs could be mined for SBPs to construct siderophore affinity resins that might enable rapid isolation of new and even cryptic siderophores from microbial cultures. Genes encoding for SBPs from metagenomic studies could be converted to siderophore affinity resins to prospect dilute metagenomic samples, including human microbiome samples.[118-121] Siderophores from probiotic and pathogenic microbes play important roles in human health.[122, 123] Detection of siderophores in patient-derived samples from the human microbiome is required for linking these microbial metabolites to biological processes relevant to mutualistic and pathogenic relationships.[124] SBP-resins might be useful for concentrating siderophores from the human microbiome with potential

applications in probiotics, pathogen diagnostics, and elucidation of important host-microbe and microbe-microbe interactions that depend on siderophores.[12, 19]

Experimental Section

Strains, materials, and instrumentation.

Staphylococcus aureus ATCC 11632 and *Streptomyces violaceus* DSM 8286 were obtained from the ATCC and DSMZ collections, respectively (**Supplementary Table 1**). *E. coli* BL21-Gold(DE3) and *E. coli* TOP10 cells were obtained from Agilent and Invitrogen, respectively. *E. coli* cells were made electrocompetent by standard methods. A Bio-Rad MicroPulser electroporator and 0.2 cm gap sterile electroporation cuvettes were used for electroporation. Bacteria were stored as frozen glycerol stocks at -80 °C. Codon-optimized *fhuD2Δ24* was purchased from GenScript in a pET28a vector for heterologous expression in *E. coli* BL21(DE3) with an *N*-terminal hexahistidine tag (**Supplementary Tables 2,3**). *N*-His_6-FhuD2Δ24 was overexpressed and purified as described previously (**Supplementary Fig. 1,2**).[31] DNA purification was performed with kits from Qiagen. Plasmid sequencing was performed by Genewiz. Nickel-nitriloacetic acid (Ni-NTA) agarose was purchased from ThermoFisher Scientific (catalog # R90115). Any *k*D SDS-PAGE gels were purchased from Bio-Rad. Proteins were dialyzed using 10K MWCO SnakeSkin dialysis tubing purchased from Thermo Fisher Scientific. Proteins were concentrated by centrifugal filrations using 30K MWCO filters from Millipore. All aqueous solutions were prepared with water purified using a Milli-Q system and sterilized by filtration through a 0.2 μm filter. Media was sterilized using an autoclave unless otherwise stated. pH measurements were recorded using an Orion Star A111 pH meter and a PerpHecT ROSS micro combination pH electrode from Thermo Fisher. All buffers, salts, media, solvents, and chemical reagents were purchased from Sigma Aldrich unless otherwise stated. All media was sterilized in an autoclave prior to growing bacteria. Siderophore samples **FO**, **SFO**, **AcFO**, and **Dan** were prepared as described previously (**Supplementary Fig. 3**).[31]

LC-MS was performed using an Agilent 6130 quadrupole with G1313 autosampler, G1315 diode array detector, and 1200 series solvent module. Samples were prepared in 0.45 μ

PTFE mini-UniPrep vials from Agilent. Separations were achieved using a 5 μ Gemini C18 column (50 x 2 mm) from Phenomenex fit with a guard column. Mobile phases were 0.1% formic acid in (A) H_2O and (B) ACN. Data were processed using G2710 ChemStation software. Preparative HPLC was performed using a Beckman Coulter SYSTEM GOLD 127P solvent module and 168 diode array detector using a Luna 10 μ C18(2) 100 Å column (250 x 21.2 mm) from Phenomenex fit with a guard column (15 x 21.2 mm). Mobile phases for RP-C18 prep-HPLC were 5 mM ammonium acetate in (A) H_2O and (B) ACN. Analytical HPLC was performed using a Beckman Coulter SYSTEM GOLD 127P solvent module and 168 detector with a Phenomenex Luna 10u C18(2) 100 Å column, 250 x 21.20 mm, 10 μm with guard column. HPLC data were processed using 32 Karat software, version 7.0. DNA and protein concentrations were determined using a NanoDrop 2000 UV–vis spectrophotometer from Thermo Fisher Scientific. Protein extinction coefficients were determined using the ExPasy ProtParam tool. UV–vis spectrophotometry was performed in 1 cm quartz cuvettes on an Agilent Cary 50 spectrophotometer. High-resolution LC-MS/MS spectra were collected using a Q-Exactive (Thermo-Fisher Scientific) equipped with a custom built Eksigent microLC at the Donald Danforth Plant Science Center, St. Louis, MO. Mobile phases were 0.1% formic acid in (A) H_2O and (B) ACN and a Supelco C8 column (0.5 x 150 mm) was used for chromatographic separations. A flow rate of 15 μL/min was held constant while a solvent gradient (2% B held for 3 min, then ramped to 100% B over 11 min, then held at 100% B for 4 min, then ramped to 2% B over 1 min, and re-equilibrated at 2% B for 6 min) was formed. The mass spectrometer was operated in polarity switching mode and scanned from *m/z* 200–500 at a resolution setting of 70,000 (at *m/z* 200) for MS_1 and a resolution of 17,500 for MS_2. Proteins were analyzed by ESI-MS using a QTOF Bruker Maxis equipped with a microLC at the WUSTL NIH/NIGMS-supported Biomedical Mass Spectrometry Research Resource. Mobile phases were 0.1% formic acid in (A) H_2O and (B) 80% H_2O/20% ACN and an Eclipse XDB-C8 (3.5 μm) column was used for chromatographic separations. A flow rate of 200 μL/min was held constant while a solvent gradient (5% B ramped to 20% B over 2 min, then ramped to 70% B over 2.5 min, then ramped to 80% B over 0.5 min and held for 1 min, then ramped to 5% B over 0.5 min, and finally ramped to 0% B over 1.5 min. The mass spectrometer was operated with a drying temperature of 180

°C, a capillary voltage of 4,000 V, and a mass range of 250–2500 *m/z*. Data was processed using Intact Mass-Protein Metrics.

FhuD2 fluorescence quenching.

FhuD2 fluorescence quenching was performed as described previously by our group.[31] Increasing concentrations of siderophore solutions in 100 nM *N*-His_6-FhuD2Δ24 in TBS buffer (25 mM Tris-HCl, 8 g/L NaCl, 0.2 g/L KCl, pH 7.4) were added over 2 min intervals to a 100 nM FhuD2 solution in TBS buffer, maintaining constant volume of 300 µL. Increments of siderophore concentrations were 0 (buffer control), 26.7, 53.2, 79.5, 105.6, 171, 299, 422, and 881 nM, or until maximum fluorescence no longer decreased. A PerkinElmer LS 55 Luminescence Spectrometer was used for all measurements. Emissions were analyzed from 300–400 nm with the following settings: the excitation wavelength was 280 nm; excitation and emission slits were both set to 10 nm; scan speed was set to 400 nm/min. Maximum fluorescence, usually around 340 nm, was taken for each siderophore concentration and dose dependent fluorescence quenching data were processed using GraphPad Prism v7.0b to calculate the apparent K_d of *N*-His_6-FhuD2Δ24 for each siderophore using a nonlinear fit to a one binding site model. A HellmaAnalytics High Precision Cell cuvette made of Quartz SUPRASIL, light path 10x2 mm was used for all experiments. Experiments were performed in triplicate as independent trials.

Siderophore purification with SBP-resin.

A fritted glass column was loaded with fresh Ni-NTA agarose resin in 1:1 EtOH:H_2O to give a working resin volume of 2.3 cm x 1 cm. The resin was washed with H_2O and equilibrated with SBP buffer (50 mM K_2HPO_4, 150 mM NaCl, 1 mM DTT, pH 8) at 4 °C. *N*-His_6-FhuD2Δ24 was thawed from a frozen stock (500 µL of 1.5 mM in SBP buffer; this is enough protein to fully saturate the Ni-NTA agarose resin), diluted to 3 mL final volume with SBP buffer, and added to the Ni-NTA agarose resin. After rocking at 4 °C for 30 min excess SBP buffer was eluted and the column was washed with SBP buffer until no *N*-His_6-FhuD2Δ24 was detected by SDS-PAGE analysis. The *N*-His_6-FhuD2Δ24-saturated Ni-NTA agarose resin is referred to as SBP-resin. Three siderophores (**FO**, **SFO**, and **AcFO**) were used in pairs as the

siderophore of interest (S_1) or sacrificial siderophore (S_2). Siderophore S_1 is first loaded to the SBP-resin by addition of 5 mL of a 0.1 mg/mL solution of S_1 in SBP buffer followed by 20 min of rocking at 4 °C. Excess SBP buffer is eluted and the SBP resin is washed five times with 15 mL of SBP buffer until LC-MS analysis shows no detectable ions for siderophore S_1. Next, 5 mL of a 0.1 mg/mL solution siderophore S_2 in SBP buffer is added and the SBP resin is rocked at 4 °C for 20 min. The column eluent is analyzed by LC-MS for the presence of siderophore S_1 ions to confirm displacement from the SBP resin by competitive binding of excess siderophore S_2. The SBP resin can now be used in a second cycle using the now resin bound siderophore S_2 as the siderophore of interest S_1. For LC-MS analysis of samples a gradient was formed from 0% B to 100% B over 10 min, followed by a 10 min hold at 100% B, and re-equilibration to 0% B over 5 min. Caution: using DTT in SBP buffer can lead to reduced Ni-NTA resin as indicated by a blue to orange color change during the procedure. BME can be used as an alternative to DTT to prevent this from taking place. Each experiment was performed in duplicate as independent trials.

Separation of siderophores by ion exchange chromatography.

A fritted glass column was packed by gravity with DEAE or Cellex P resin giving a working resin volume of 2 cm x 7 cm. Resins were washed with 50 mL of 10 mM ammonium acetate solution in H_2O (pH 7) followed by 50 mL of pure H_2O. For proof-of-principle studies, 1:1 mixtures of iron(III)-bound siderophores (**FO + SFO**; **SFO + AcFO**; **FO + AcFO**) at 0.1 mg/mL for each siderophore were prepared in pure H_2O. Samples from SBP-resin elutions containing combinations of siderophores at ~0.1 mg/mL each were first desalted and then reconstituted in pure H_2O. Desalting was accomplished by either lyophilization followed by trituration with MeOH or C18 chromatography. A 5 mL aliquot of **FO + SFO** solution was passed through DEAE resin. The flowthrough was collected (contains **FO**) and the column was washed with 2 x 5 mL pure H_2O. **SFO** was eluted from the DEAE resin using 5 mL of 4% aqueous NH_4OH. A 5 mL aliquot of **SFO + AcFO** solution was passed through DEAE resin. The flow-through was collected (contains **AcFO**) and the column was washed with 2 x 5 mL pure H_2O. **SFO** was eluted from the DEAE resin using 5 mL of 4% aqueous NH_4OH. A 5 mL aliquot of **FO + AcFO** was passed through Cellex P resin. The flow-through was collected (contains **AcFO**) and the column was washed with 2 x 5 mL pure H_2O. **FO** was eluted from

the Cellex P resin using 5 mL of 4% aqueous NH_4OH. For each separation, the column load, flowthrough, washes, and elution were analyzed by LC-MS. Each separation was performed in duplicate as independent trials.

Purification of salmycins from S. violaceus DSM 8286.

Salmycins A–D (**Sal A–D**) were purified from cultures of *Streptomyces violaceus* DSM 8286 (**Supplementary Table 1**; **Supplementary Fig. 6**).[103, 112, 113] Spore stocks of *S. violaceus* DSM 8286 were grown on malt extract agar plates (10 g/L starch, 1 g/L casein, 1 g/L peptone, 1 g/L yeast extract, 10 g/L malt extract, 0.5 g/L K_2HPO_4, 15 g/L agar) at 28 °C for 7–10 days, or until spores were formed. A liquid culture was started by adding a 1 cm^2 slice from the agar plate to 250 mL of liquid growth media (15 g/L glucose, 15 g/L soy bean flour, 5 mL/L corn steep liquor, 2 g/L $CaCO_3$, and 5 g/L NaCl, pH adjusted to 7.2) in a 1 L baffled flask. The starter culture was incubated at 28 °C with shaking at 225 r.p.m for 48 h. 50 mL of starter culture was transferred to a 3 L baffled flask containing 1 L of salmycin production media (20 g/L soy bean flour and 20 g/L mannitol, pH adjusted to 7.5). Salmycin production cultures were incubated with shaking at 225 r.p.m. at 28 °C for 4 days. Salmycin production was monitored by antibacterial susceptibility testing against *S. aureus* ATCC 11632, as described below. Cultures (10 L total volume) were vacuum filtered through celite and concentrated by rotary evaporation. The resulting solids were washed with a 90% MeOH/10% H_2O solution (v/v) several times. The combined MeOH washings were concentrated by rotary evaporation and dissolved in 10 mL of pure H_2O. A pure mixture of salmycins A–D can be obtained using *N*-His_6-FhuD2Δ24 SBP-resin as described previously using the salmycins as siderophore S_1 and **FO**, **SFO**, **AcFO**, or **Dan** as siderophore S_2. **Dan** is advantageous as siderophore S_2 because it offers the greatest separation from the salmycins by RP-C18 HPLC (**Supplementary Fig. 8**).

For preparative scale purification of salmycins A–D we employed the use of centrifugal filtration with soluble *N*-His_6-FhuD2Δ24 rather than Ni-NTA-immobilized protein. Culture supernatant (5 L total volume) from *S. violaceus* DSM 8286 production cultures was passed through a column of hydrophobic HP-20 resin (6 cm wide x 25 cm high) to absorb the salmycins. The HP-20 resin was washed with H_2O and the crude salmycins were eluted

from the HP-20 resin by the addition of a 20% IPA/80% H_2O. The IPA/H_2O were removed via rotary evaporation to give a dark brown solid. The solid was suspended in a minimal volume of 90% MeOH/10% H_2O and then centrifuged at 5,000 r.p.m. at 4 °C for 20 min. The supernatant was collected and the solid was treated with 90% MeOH/10% H_2O a second time. The supernatants were combined and concentrated by rotary evaporation to give an orange solid. The solid was dissolved in H_2O and filtered through a DEAE anion exchange column (2 cm wide x 7 cm high). The flowthrough from the DEAE resin was concentrated and dissolved in SBP buffer. This solution is suitable for siderophore-affinity chromatography using immobilized SBP columns (**Supplementary Fig. 7**), as described previously, or soluble SBP centrifugal filtration units. For the centrifugal filtration protocol using soluble SBP, eight Amicon Ultra 30K MWCO centrifugal filters were filled with 250 µL of 800 µM *N*-His_6-FhuD2Δ24 diluted to 1 mL total volume in SBP buffer. Approximately 15 mL of crude salmycins in SBP buffer was added to each centrifugal filter and rocked at 4 °C for 30 min. Each centrifugal filter was then centrifuged at 5,000 r.p.m. at 4 °C for 15 min or until ~1-2 mL of volume remained in the filtration unit. An additional 15 mL of crude salmycin solution in SBP buffer was added to each tube and the process was repeated until all of the crude salmycin solution was passed through the *N*-His_6-FhuD2Δ24 centrifugal filters. To elute the pure salmycins, a 5 mL solution of 0.2 mg/L **Dan** in SBP buffer was added to each centrifugal filter. After rocking for 30 min at 4 °C, the solutions were centrifuged at 5,000 r.p.m. and the flowthrough was collected. An additional 5 mL of SBP buffer was added to each centrifugal filter and the flowthrough after centrifugation was combined with the previous flowthrough to give ~10 mL total volume from each centrifugal filter. The flowthroughs from all centrifugal filtration units were combined and concentrated via rotary evaporation to yield an orange solid. To decrease the salt content, the solid was suspended in 90% MeOH/10% H_2O and filtered. The remaining solid was washed several times with 90% MeOH/10% H_2O and the pooled MeOH/H_2O washings were concentrated via rotary evaporation and redissolved in H_2O. HPLC and LC-MS analysis revealed a mixture of **Dan** and salmycins A–D that was separated using preparative RP-C18 HPLC using a gradient of 5% B held for 2 min, ramped to 25% B over 5 min, then 45% B over 20 min, and 100% over 3 min followed by re-equilibration to 0% B

over 2 min (**Supplementary Fig. 8**). Danoxamine eluted from 15–16 min and salmycins A–D were collected from 16–20 min. Fractions containing the salmycins were confirmed by bioactivity, analytical RP-C18 HPLC, LC-MS, and high-resolution LC-MS/MS (**Supplementary Fig. 9–11**). This resulted in a solution of analytically pure salmycins A–D with a total volume of 500 µL and a total concentration of 81 µM (42 µg), which enabled the determination of apparent K_{Fe}, apparent *N*-His_6-FhuD2Δ24 K_d, and *S. aureus* MIC values.

Determination of salmycin K_{Fe}.

The apparent K_{Fe} value for the purified mixture of salmycins A–D was measured using an EDTA competition assay for 1:1 siderophore:Fe(III) complexes described previously by our group (**Supplmentary Fig. 13c**).[31] A solution of pure salmycins at 0.1 µM was mixed with 1.2 equivalents of EDTA in HEPES buffer (10 mM HEPES, 600 mM NaCl, 100 mM KCl, adjusted to pH 7.4) to a total volume of 1 mL. The solution was transferred to a polypropylene cuvette and scanned continuously at 430 nm over 90 min at 1 s/scan. The experiment was performed in duplicate as independent trials. Apparent K_{Fe} was calculated from the change in absorbance at 430 nm as described previously.[31]

Antibacterial susceptibility testing.

Antibacterial activity of the salmycins was determined by an agar diffusion assay or liquid broth microdilution assay. For both assays, overnight cultures of *S. aureus* ATCC 11632 were grown in LB broth for 18–24 h starting from a frozen glycerol stock. For the agar diffusion assay, 40 µL of this culture was added to 34 mL of sterile, melted, and tempered (~47 °C) Mueller-Hinton No. 2 agar (HiMedia Laboratories) supplemented with 100 µM 2,2'-bipyridine (final concentration). After gentle mixing, the inoculated melted agar was poured into a sterile petri dish (145 mm x 20 mm, Greiner Bio-One) and allowed to solidify at rt. Wells of 9 mm diameter were cut from the petri dish agar and filled with 50 µL of the test sample solution. All pure test samples (**FO**, salmycins, and **Dan**) were tested at concentrations of 0.1 mg/mL. For testing of crude salmycins during purification the concentration was unknown and antibacterial activity against *S. aureus* was used as a qualitative measurement for the presence of the salmycins. The petri dish was incubated at 37 °C in ambient air for 18–24 h and the inhibition zone diameters were measured (mm)

with an electronic caliper. MIC values were determined using the broth microdilution strategy following CLSI guidelines in Mueller-Hinton No. 2 broth supplemented with 100 μM 2,2'-bipyridine, as described previously by our group.[31, 33] A concentration gradient of 1–0.0002 μM salmycins was used and an MIC value of 7.8 nM was recorded for halting growth of *S. aureus* ATCC 11632 after 18 h incubation at 37 °C in ambient air. The MIC was judged visually as the lowest salmycin concentration to completely inhibit the growth of *S. aureus* ATCC 11632.

Associated Content

Supplementary figures, supplementary tables, SDS protein gels, high-resolution mass spectra, compound purity analysis, FhuD2 fluorescence quenching plots, K_{Fe} measurements, and antibacterial susceptibility testing. The Supporting Information is available free of charge on the ACS Publications website at http://pubs.acs.org.

Corresponding Author

*Timothy A. Wencewicz; E-mail: wencewicz@wustl.edu; Ph: 314-935-7247; Fax: 314-935-6530; ORCID: 0000-0002-5839-6672

Funding

Research was supported by start-up funds from Washington University in St. Louis, Oak Ridge Associated Universities via a Ralph E. Powe Junior Faculty Enhancement Award FY2014-215, and NSF CAREER Award 1654611 to T.A.W.

Notes

The authors declare no competing financial interest.

Acknowledgements

We thank Dr. Brad Evans at the Proteomics & Mass Spectrometry Facility at the Donald Danforth Plant Science Center, St. Louis, MO for assistance with the acquisition of the QTRAP LC-MS/MS spectra (supported by the National Science Foundation under Grant No. DBI-0521250). We thank Prof. John-Stephen Taylor (WUSTL, Dept. of Chemistry) for assistance with fluorescence quenching studies. We thank Prof. Marvin J. Miller (University of Notre Dame, Dept. of Chemistry and Biochemistry) for providing samples of **SFO** and **Dan** through an MTA. We thank Prof. Michael Gross and Ming Cheng (WUSTL, Dept. of Chemistry; NIH P41GM103422) for assistance with ESI-MS analysis of *N*-His_6-FhuD2Δ24.

Abbreviations

AcFO, acetyl ferrioxamine; ACN, acetonitrile; ASMS, affinity selection-mass spectrometry; BME, β-mercaptoethanol; CLSI, Clinical and Laboratory Standards Institute; DTT, dithiothreitol; ESI, electrospray ionization; FO, ferrioxamine; FPLC, fast protein liquid chromatography; His_6, hexahistidine; HPLC, high-performance liquid chromatography; IPA, isopropyl alcohol; LB, Luria Broth; LC-MS, liquid chromatography-mass spectrometry; MIC, minimum inhibitory concentration; MWCO, molecular weight cut-off; MTA, material transfer agreement; Ni-NTA, nickel nitrilotriacetic acid agarose; PBP, periplasmic binding protein; r.p.m., rotations per minute; rt, room temperature; S_1, siderophore 1; S_2 siderophore 2; SAC, siderophore-antibiotic conjugate; Sal, salmycin; SBP, siderophore-binding protein; SDS, sodium dodecyl sulfate; SFO, succinoyl ferrioxamine.

References

[1] Newman, D. J., and Cragg, G. M. (2016) Natural products as sources of new drugs from 1981 to 2014, *J. Nat. Prod. 79*, 629-661. DOI: 10.1126/science.125476610.1021/acs.jnatprod.5b01055

[2] Wencewicz, T. A. (2016) New antibiotics from nature's chemical inventory, *Bioorg. Med. Chem. 24*, 6227-6252. DOI: 10.1016/j.bmc.2016.09.014

[3] Neilands, J. B. (1995) Siderophores: Structure and function of microbial iron transport compounds, *J. Biol. Chem. 270*, 26723-26726. DOI: 10.1074/jbc.270.45.26723

[4] Hider, R. C., and Kong, X. (2010) Chemistry and biology of siderophores, *Nat. Prod. Rep. 27*, 637-657. DOI: 10.1039/B906679A

[5] Raymond, K. N., Allred, B. E., and Sia, A. K. (2015) Coordination chemistry of microbial iron transport, *Acc. Chem. Res. 48*, 2496-2505. DOI: 10.1021/acs.accounts.5b00301
[6] Kalinowski, D. S., and Richardson, D. R. (2005) The evolution of iron chelators for the treatment of iron overload disease and cancer, *Pharmacol. Rev. 57*, 547-583. DOI: 10.1124/pr.57.4.2
[7] Codd, R., Richardson-Sanchez, T., Telfer, T. J., and Gotsbacher, M. P. (2018) Advances in the chemical biology of desferrioxamine B, *ACS Chem*. *Biol. 13*, 11-25. DOI: 10.1021/acschembio.7b00851
[8] Cloonan, S. M., Glass, K., Laucho-Contreras, M. E., Bhashyam, A. R., Cervo, M., Pabon, M. A., Konrad, C., Polverino, F., Siempos, II, Perez, E., Mizumura, K., Ghosh, M. C., Parameswaran, H., Williams, N. C., Rooney, K. T., Chen, Z. H., Goldklang, M. P., Yuan, G. C., Moore, S. C., Demeo, D. L., Rouault, T. A., D'Armiento, J. M., Schon, E. A., Manfredi, G., Quackenbush, J., Mahmood, A., Silverman, E. K., Owen, C. A., and Choi, A. M. (2016) Mitochondrial iron chelation ameliorates cigarette smoke-induced bronchitis and emphysema in mice, *Nat. Med. 22*, 163-174. DOI: 10.1038/nm.4021
[9] Tchanque-Fossuo, C. N., Dahle, S. E., Buchman, S. R., and Rivkah Isseroff, R. (2017) Deferoxamine: potential novel topical therapeutic for chronic wounds, *Br. J. Dermatol. 176*, 1056-1059. DOI: 10.1111/bjd.14956
[10] Shanzer, A., Libman, J., Lytton, S. D., Glickstein, H., and Cabantchik, Z. I. (1991) Reversed siderophores act as antimalarial agents, *Proc. Natl. Acad. Sci. U. S. A. 88*, 6585-6589. DOI: 10.1073/pnas.88.15.6585
[11] Yamasaki, T., Terai, S., and Sakaida, I. (2011) Deferoxamine for advanced hepatocellular carcinoma, *N. Engl. J. Med. 365*, 576-578. DOI: 10.1056/NEJMc1105726
[12] Johnstone, T. C., and Nolan, E. M. (2015) Beyond iron: Non-classical biological functions of bacterial siderophores, *Dalton Trans. 44*, 6320-6339. DOI: 10.1039/C4DT03559C
[13] Troxell, B., and Hassan, H. M. (2013) Transcriptional regulation by ferric uptake regulator (Fur) in pathogenic bacteria, *Front. Cell Infect. Microbiol. 3*, 59. DOI: 10.3389/fcimb.2013.00059
[14] Crosa, J. H., and Walsh, C. T. (2002) Genetics and assembly line enzymology of siderophore biosynthesis in bacteria, *Microbiol. Mol. Biol. Rev. 66*, 223-249. DOI: 10.1128/MMBR.66.2.223-249.2002
[15] Hannauer, M., Yeterian, E., Martin, L. W., Lamont, I. L., and Schalk, I. J. (2010) An efflux pump is involved in secretion of newly synthesized siderophore by *Pseudomonas aeruginosa*, *FEBS Lett. 584*, 4751-4755. DOI: 10.1016/j.febslet.2010.10.051
[16] Celia, H., Noinaj, N., Zakharov, S. D., Bordignon, E., Botos, I., Santamaria, M., Barnard, T. J., Cramer, W. A., Lloubes, R., and Buchanan, S. K. (2016) Structural insight into the role of the Ton complex in energy transduction, *Nature 538*, 60-65. DOI: 10.1038/nature19757
[17] Clarke, T. E., Ku, S. Y., Dougan, D. R., Vogel, H. J., and Tari, L. W. (2000) The structure of the ferric siderophore binding protein FhuD complexed with gallichrome, *Nat. Struct. Biol. 7*, 287-291. DOI: 10.1038/74048
[18] Korkhov, V. M., Mireku, S. A., and Locher, K. P. (2012) Structure of AMP-PNP-bound vitamin B12 transporter BtuCD–F, *Nature 490*, 367. DOI: 10.1038/nature11442

[19] Miethke, M., and Marahiel, M. A. (2007) Siderophore-based iron acquisition and pathogen control, *Microbiol. Mol. Biol. Rev. 71*, 413-451. DOI: 10.1128/MMBR.00012-07

[20] Miethke, M. (2013) Molecular strategies of microbial iron assimilation: from high-affinity complexes to cofactor assembly systems, *Metallomics 5*, 15-28. DOI: 10.1039/C2MT20193C

[21] Li, K., Chen, W.-H., and Bruner, S. D. (2015) Structure and Mechanism of the Siderophore-Interacting Protein from the Fuscachelin Gene Cluster of Thermobifida fusca, *Biochemistry 54*, 3989-4000. DOI: 10.1021/acs.biochem.5b00354

[22] Kobylarz, M. J., Heieis, G. A., Loutet, S. A., and Murphy, M. E. P. (2017) Iron uptake oxidoreductase (IruO) uses a flavin adenine dinucleotide semiquinone intermediate for iron-siderophore reduction, *ACS Chem. Biol. 12*, 1778-1786. DOI: 10.1021/acschembio.7b00203

[23] Imperi, F., Tiburzi, F., and Visca, P. (2009) Molecular basis of pyoverdine siderophore recycling in *Pseudomonas aeruginosa*, *Proc. Natl. Acad. Sci. U. S. A. 106*, 20440-20445. DOI: 10.1073/pnas.0908760106

[24] Yeterian, E., Martin, L. W., Lamont, I. L., and Schalk, I. J. (2010) An efflux pump is required for siderophore recycling by *Pseudomonas aeruginosa*, *Environ. Microbiol. Rep. 2*, 412-418. DOI: 10.1111/j.1758-2229.2009.00115.x

[25] Koh, E. I., Robinson, A. E., Bandara, N., Rogers, B. E., and Henderson, J. P. (2017) Copper import in *Escherichia coli* by the yersiniabactin metallophore system, *Nat. Chem. Biol. 13*, 1016-1021. DOI: 10.1038/nchembio.2441

[26] Nakaminami, H., Chen, C., Truong-Bolduc, Q. C., Kim, E. S., Wang, Y., and Hooper, D. C. (2017) Efflux transporter of siderophore staphyloferrin A in *Staphylococcus aureus* contributes to bacterial fitness in abscesses and epithelial cells, *Infect. Immun. 85*, e00358-17. DOI: 10.1128/IAI.00358-17

[27] Ganne, G., Brillet, K., Basta, B., Roche, B., Hoegy, F., Gasser, V., and Schalk, I. J. (2017) Iron release from the siderophore pyoverdine in *Pseudomonas aeruginosa* involves three new actors: FpvC, FpvG, and FpvH, *ACS Chem. Biol. 12*, 1056-1065. DOI: 10.1021/acschembio.6b01077

[28] Lin, H., Fischbach, M. A., Liu, D. R., and Walsh, C. T. (2005) In vitro characterization of salmochelin and enterobactin trilactone hydrolases IroD, IroE, and Fes, *J. Am. Chem. Soc. 127*, 11075-11084. DOI: 10.1021/ja0522027

[29] Sheldon, J. R., and Heinrichs, D. E. (2015) Recent developments in understanding the iron acquisition strategies of gram positive pathogens, *FEMS Microbiol. Rev. 39*, 592-630. DOI: 10.1093/femsre/fuv009

[30] D'Onofrio, A., Crawford, J. M., Stewart, E. J., Witt, K., Gavrish, E., Epstein, S., Clardy, J., and Lewis, K. (2010) Siderophores from neighboring organisms promote the growth of uncultured bacteria, *Chem. Biol. 17*, 254-264. DOI: 10.1016/j.chembiol.2010.02.010

[31] Endicott, N. P., Lee, E., and Wencewicz, T. A. (2017) Structural basis for xenosiderophore utilization by the human pathogen *Staphylococcus aureus*, *ACS Infect. Dis. 3*, 542-553. DOI: 10.1021/acsinfecdis.7b00036

[32] Braun, V., Pramanik, A., Gwinner, T., Koberle, M., and Bohn, E. (2009) Sideromycins: tools and antibiotics, *Biometals 22*, 3-13. DOI: 10.1007/s10534-008-9199-7

[33] Wencewicz, T. A., Long, T. E., Möllmann, U., and Miller, M. J. (2013) Trihydroxamate siderophore–fluoroquinolone conjugates are selective sideromycin antibiotics that target *Staphylococcus aureus*, *Bioconjugate Chem. 24*, 473-486. DOI: 10.1021/bc300610f

[34] Wencewicz, T. A., and Miller, M. J. (2017) Sideromycins as pathogen-targeted antibiotics. In: *Topics in Medicinal Chemistry*, Springer, Berlin, Heidelberg. DOI: 10.1007/7355 2017 19. DOI: 10.1007/7355 2017 19

[35] Galet, J., Deveau, A., Hotel, L., Frey-Klett, P., Leblond, P., and Aigle, B. (2015) *Pseudomonas fluorescens* pirates both ferrioxamine and ferricoelichelin siderophores from *Streptomyces ambofaciens*, *Appl. Environ. Microbiol. 81*, 3132-3141. DOI: 10.1128/AEM.03520-14

[36] Boiteau, R. M., Mende, D. R., Hawco, N. J., McIlvin, M. R., Fitzsimmons, J. N., Saito, M. A., Sedwick, P. N., DeLong, E. F., and Repeta, D. J. (2016) Siderophore-based microbial adaptations to iron scarcity across the eastern Pacific Ocean, *Proc. Natl. Acad. Sci. U. S. A. 113*, 14237-14242. DOI: 10.1073/pnas.1608594113

[37] Ejje, N., Soe, C. Z., Gu, J., and Codd, R. (2013) The variable hydroxamic acid siderophore metabolome of the marine actinomycete *Salinispora tropica* CNB-440, *Metallomics 5*, 1519-1528. DOI: 10.1039/C3MT00230F

[38] Codd, R. (2008) Traversing the coordination chemistry and chemical biology of hydroxamic acids, *Coord. Chem. Rev. 252*, 1387-1408. DOI: 10.1016/j.ccr.2007.08.001

[39] Barona-Gomez, F., Wong, U., Giannakopulos, A. E., Derrick, P. J., and Challis, G. L. (2004) Identification of a cluster of genes that directs desferrioxamine biosynthesis in *Streptomyces coelicolor* M145, *J. Am. Chem. Soc. 126*, 16282-16283. DOI: 10.1021/ja045774k

[40] Telfer, T. J., Gotsbacher, M. P., Soe, C. Z., and Codd, R. (2016) Mixing up the pieces of the desferrioxamine B jigsaw defines the biosynthetic sequence catalyzed by DesD, *ACS Chem. Biol. 11*, 1452-1462. DOI: 10.1021/acschembio.6b00056

[41] Challis, G. L. (2005) A widely distributed bacterial pathway for siderophore biosynthesis independent of nonribosomal peptide synthetases, *Chembiochem 6*, 601-611. DOI: 10.1002/cbic.200400283

[42] Kadi, N., Oves-Costales, D., Barona-Gomez, F., and Challis, G. L. (2007) A new family of ATP-dependent oligomerization-macrocyclization biocatalysts, *Nat. Chem. Biol. 3*, 652-656. DOI: 10.1038/nchembio.2007.23

[43] Salomone-Stagni, M., Bartho, J. D., Polsinelli, I., Bellini, D., Walsh, M. A., Demitri, N., and Benini, S. (2018) A complete structural characterization of the desferrioxamine E biosynthetic pathway from the fire blight pathogen *Erwinia amylovora*, *J. Struct. Biol*. ASAP, Feb. 8, DOI: 10.1016/j.jsb.2018.02.002

[44] Lewis, K., Epstein, S., D'Onofrio, A., and Ling, L. L. (2010) Uncultured microorganisms as a source of secondary metabolites, *J. Antibiot. 63*, 468-476. DOI: 10.1038/ja.2010.87

[45] Rutledge, P. J., and Challis, G. L. (2015) Discovery of microbial natural products by activation of silent biosynthetic gene clusters, *Nat. Rev. Microbiol. 13*, 509. DOI: 10.1038/nrmicro3496

[46] Schwyn, B., and Neilands, J. B. (1987) Universal chemical assay for the detection and determination of siderophores, *Anal. Biochem. 160*, 47-56. DOI: 10.1016/0003-2697(87)90612-9

[47] Louden, B. C., Haarmann, D., and Lynne, A. M. (2011) Use of blue agar CAS assay for siderophore detection, *J. Microbiol. Biol. Educ. 12*, 51-53. DOI: 10.1128/jmbe.v12i1.249

[48] Baars, O., Zhang, X., Morel, F. M. M., and Seyedsayamdost, M. R. (2016) The siderophore metabolome of *Azotobacter vinelandii*, *Appl. Environ. Microbiol. 82*, 27-39. DOI: 10.1128/AEM.03160-15

[49] Sidebottom, A. M., Johnson, A. R., Karty, J. A., Trader, D. J., and Carlson, E. E. (2013) Integrated metabolomics approach facilitates discovery of an unpredicted natural product suite from *Streptomyces coelicolor* M145, *ACS Chem. Biol. 8*, 2009-2016. DOI: 10.1021/cb4002798

[50] Adnani, N., Chevrette, M. G., Adibhatla, S. N., Zhang, F., Yu, Q., Braun, D. R., Nelson, J., Simpkins, S. W., McDonald, B. R., Myers, C. L., Piotrowski, J. S., Thompson, C. J., Currie, C. R., Li, L., Rajski, S. R., and Bugni, T. S. (2017) Coculture of marine invertebrate-associated bacteria and interdisciplinary technologies enable biosynthesis and discovery of a new antibiotic, keyicin, *ACS Chem. Biol. 12*, 3093-3102. DOI: 10.1021/acschembio.7b00688

[51] Smanski, M. J., Zhou, H., Claesen, J., Shen, B., Fischbach, M. A., and Voigt, C. A. (2016) Synthetic biology to access and expand nature's chemical diversity, *Nat. Rev. Microbiol. 14*, 135-149. DOI: 10.1038/nrmicro.2015.24

[52] Amos, G. C. A., Awakawa, T., Tuttle, R. N., Letzel, A.-C., Kim, M. C., Kudo, Y., Fenical, W., S. Moore, B., and Jensen, P. R. (2017) Comparative transcriptomics as a guide to natural product discovery and biosynthetic gene cluster functionality, *Proc. Natl. Acad. Sci. U. S. A. 114*, E11121-E11130. DOI: 10.1073/pnas.1714381115.

[53] Smith, T. E., Pond, C. D., Pierce, E., Harmer, Z. P., Kwan, J., Zachariah, M. M., Harper, M. K., Wyche, T. P., Matainaho, T. K., Bugni, T. S., Barrows, L. R., Ireland, C. M., and Schmidt, E. W. (2018) Accessing chemical diversity from the uncultivated symbionts of small marine animals, *Nat. Chem. Biol*. *14*, 179-185. DOI: 10.1038/nchembio.2537

[54] Charlop-Powers, Z., Milshteyn, A., and Brady, S. F. (2014) Metagenomic small molecule discovery methods, *Curr. Opin. Microbiol. 19*, 70-75. DOI: 10.1016/j.mib.2014.05.021

[55] Dejong, C. A., Chen, G. M., Li, H., Johnston, C. W., Edwards, M. R., Rees, P. N., Skinnider, M. A., Webster, A. L., and Magarvey, N. A. (2016) Polyketide and nonribosomal peptide retro-biosynthesis and global gene cluster matching, *Nat. Chem. Biol. 12*, 1007-1014. DOI: 10.1038/nchembio.2188

[56] Zlitni, S., Ferruccio, L. F., and Brown, E. D. (2013) Metabolic suppression identifies new antibacterial inhibitors under nutrient limitation, *Nat. Chem. Biol. 9*, 796-804. DOI: 10.1038/nchembio.1361

[57] Covington, B. C., McLean, J. A., and Bachmann, B. O. (2017) Comparative mass spectrometry-based metabolomics strategies for the investigation of microbial secondary metabolites, *Nat. Prod. Rep. 34*, 6-24. DOI: 10.1039/C6NP00048G

[58] Challis, G. L., and Ravel, J. (2000) Coelichelin, a new peptide siderophore encoded by the *Streptomyces coelicolor* genome: structure prediction from the sequence of its non-ribosomal peptide synthetase, *FEMS Microbiol. Lett. 187*, 111-114. DOI: 10.1111/j.1574-6968.2000.tb09145.x

[59] Zhang, F., Barns, K., Hoffmann, F. M., Braun, D. R., Andes, D. R., and Bugni, T. S. (2017) Thalassosamide, a siderophore discovered from the marine-derived bacterium *Thalassospira profundimaris*, *J. Nat. Prod. 80*, 2551-2555. DOI: 10.1021/acs.jnatprod.7b00328

[60] Bruns, H., Crusemann, M., Letzel, A. C., Alanjary, M., McInerney, J. O., Jensen, P. R., Schulz, S., Moore, B. S., and Ziemert, N. (2018) Function-related replacement of bacterial siderophore pathways, *ISME J. 12*, 320-329. DOI: 10.1038/ismej.2017.137

[61] Baars, O., Zhang, X., Gibson, M. I., Stone, A. T., Morel, F. M. M., and Seyedsayamdost, M. R. (2017) Crochelins: siderophores with an iron-chelating moiety from the nitrogen-fixing bacterium *Azotobacter chroococcum*, *Angew. Chem. Int. Ed. Engl. 57*, 536-541. DOI: 10.1002/anie.201709720

[62] Mike, L. A., Tripathi, A., Blankenship, C. M., Saluk, A., Schultz, P. J., Tamayo-Castillo, G., Sherman, D. H., and Mobley, H. L. T. (2017) Discovery of nicoyamycin A, an inhibitor of uropathogenic *Escherichia coli* growth in low iron environments, *Chem. Comm. 53*, 12778-12781. DOI: 10.1039/c7cc07732g

[63] Rudolf, J. D., Dong, L.-B., and Shen, B. (2017) Platensimycin and platencin: Inspirations for chemistry, biology, enzymology, and medicine, *Biochem. Pharmacol. 133*, 139-151. DOI: 10.1016/j.bcp.2016.11.013

[64] Koehn, F. E., and Carter, G. T. (2005) The evolving role of natural products in drug discovery, *Nat. Rev. Drug Discov. 4*, 206-220. DOI: 10.1038/nrd1657

[65] Carlson, E. E., and Cravatt, B. F. (2007) Chemoselective probes for metabolite enrichment and profiling, *Nature Methods 4*, 429-435. DOI: 10.1038/nmeth1038

[66] Odendaal, A. Y., Trader, D. J., and Carlson, E. E. (2011) Chemoselective enrichment for natural products discovery, *Chem. Sci. 2*, 760-764. DOI: 10.1039/C0SC00620C

[67] Brooks, W. L., and Sumerlin, B. S. (2016) Synthesis and applications of boronic acid-containing polymers: From materials to medicine, *Chem. Rev. 116*, 1375-1397. DOI: 10.1021/acs.chemrev.5b00300

[68] Trader, D. J., and Carlson, E. E. (2011) Siloxyl ether functionalized resins for chemoselective enrichment of carboxylic acids, *Org. Lett. 13*, 5652-5655. DOI: 10.1021/ol202376m

[69] Carlson, E. E., and Cravatt, B. F. (2007) Enrichment tags for enhanced-resolution profiling of the polar metabolome, *J. Am. Chem. Soc. 129*, 15780-15782. DOI: 10.1021/ja0779506

[70] Capehart, S. L., and Carlson, E. E. (2016) Mass spectrometry-based assay for the rapid detection of thiol-containing natural products, *Chem. Comm. 52*, 13229-13232. DOI: 10.1039/C6CC07111B

[71] Siegel, D., Andrae, K., Proske, M., Kochan, C., Koch, M., Weber, M., and Nehls, I. (2010) Dynamic covalent hydrazine chemistry as a selective extraction and cleanup technique for the quantification of the Fusarium mycotoxin zearalenone in edible oils, *J. Chromatogr. A 1217*, 2206-2215. DOI: 10.1016/j.chroma.2010.02.019

[72] Krchnak, V., Moellmann, U., Dahse, H. M., and Miller, M. J. (2008) Solid-supported nitroso hetero diels-alder reactions. 2. Arylnitroso dienophiles: scope and limitations, *J. Combinator. Chem. 10*, 104-111. DOI: 10.1021/cc7001414

[73] Krchnak, V., Waring, K. R., Noll, B. C., Moellmann, U., Dahse, H. M., and Miller, M. J. (2008) Evolution of natural product scaffolds by acyl- and arylnitroso hetero-diels-

alder reactions: new chemistry on piperine, *J. Org. Chem. 73*, 4559-4567. DOI: 10.1021/jo8004827

[74] Krchnak, V., Zajicek, J., Miller, P. A., and Miller, M. J. (2011) Selective molecular sequestration with concurrent natural product functionalization and derivatization: from crude natural product extracts to a single natural product derivative in one step, *J. Org. Chem. 76*, 10249-10253. DOI: 10.1021/jo201361s

[75] Robles, O., and Romo, D. (2014) Chemo- and site-selective derivatizations of natural products enabling biological studies, *Nat. Prod. Rep. 31*, 318-334. DOI: 10.1039/c3np70087a

[76] Siegel, D. (2012) Applications of reversible covalent chemistry in analytical sample preparation, *Analyst 137*, 5457-5482. DOI: 10.1039/C2AN35697J

[77] Braich, N., and Codd, R. (2008) Immobilised metal affinity chromatography for the capture of hydroxamate-containing siderophores and other Fe(III)-binding metabolites directly from bacterial culture supernatants, *Analyst 133*, 877-880. DOI: 10.1039/B802355G

[78] Barnes, H. H., and Ishimaru, C. A. (1999) Purification of catechol siderophores by boronate affinity chromatography: Identification of chrysobactin from *Erwinia carotovora* subsp. *carotovora*, *Biometals 12*, 83-87. DOI: 10.1023/A:1009223615607

[79] Cuatrecasas, P. (1970) Protein purification by affinity chromatography: Derivatizations of agarose and polyacrylamide beads, *J. Biol. Chem. 245*, 3059-3065.

[80] Hofmann, K., and Kiso, Y. (1976) An approach to the targeted attachment of peptides and proteins to solid supports, *Proc. Natl. Acad. Sci. U. S. A. 73*, 3516-3518.

[81] Folena-Wasserman, G., Sitrin, R. D., Chapin, F., and Snader, K. M. (1987) Affinity chromatography of glycopeptide antibiotics, *J. Chromatogr. 392*, 225-238. DOI: 10.1016/S0021-9673(01)94268-2

[82] Chen, Y., Chen, Z., and Wang, Y. (2015) Immobilized magnetic beads-based multi-target affinity selection coupled with HPLC-MS for screening active compounds from traditional Chinese medicine and natural products, In: *Affinity Chromatography: Methods and Protocols* (Reichelt, S., Ed.), pp 121-129, Springer, New York, NY. DOI: 10.1016/j.jpba.2013.02.024

[83] Walker, S. S., Degen, D., Nickbarg, E., Carr, D., Soriano, A., Mandal, M., Painter, R. E., Sheth, P., Xiao, L., Sher, X., Murgolo, N., Su, J., Olsen, D. B., Ebright, R. H., and Young, K. (2017) Affinity selection–mass spectrometry identifies a novel antibacterial RNA polymerase inhibitor, *ACS Chem. Biol. 12*, 1346-1352. DOI: 10.1021/acschembio.6b01133

[84] Evans, M. J., Saghatelian, A., Sorensen, E. J., and Cravatt, B. F. (2005) Target discovery in small-molecule cell-based screens by in situ proteome reactivity profiling, *Nat. Biotechnol. 23*, 1303. DOI: 10.1038/nbt1149

[85] McFedries, A., Schwaid, A., and Saghatelian, A. (2013) Methods for the elucidation of protein-small molecule interactions, *Chem. Biol. 20*, 667-673. DOI: 10.1016/j.chembiol.2013.04.008

[86] Bugdahn, N., Peuckert, F., Albrecht, A. G., Miethke, M., Marahiel, M. A., and Oberthür, M. (2010) Direct identification of a siderophore import protein using synthetic petrobactin ligands, *Angew. Chem. Int. Ed. Engl. 49*, 10210-10213. DOI: 10.1016/j.chembiol.2011.05.006

[87] Crumbliss, A. L., Garrison, J. M., Bock, C. R., Schaaf, A., Bonaventura, C. J., and Bonaventura, J. (1987) Synthesis and characterization of iron(llI) chelating analogues of siderophores on organic solid supports, *Inorganica Chim. Acta 133*, 281-287. DOI: 10.1016/S0020-1693(00)87780-4

[88] Maier, G. P., and Butler, A. (2017) Siderophores and mussel foot proteins: the role of catechol, cations, and metal coordination in surface adhesion, *J. Biol. Inorg. Chem. 22*, 739-749. DOI: 10.1007/s00775-017-1451-6

[89] Doorneweerd, D. D., Henne, W. A., Reifenberger, R. G., and Low, P. S. (2010) Selective capture and identification of pathogenic bacteria using an immobilized siderophore, *Langmuir 26*, 15424-15429. DOI: 10.1021/la101962w

[90] Wolfenden, M., Sakamuri, R., Anderson, A., Prasad, L., Schmidt, J., and Mukundan, H. (2012) Determination of bacterial viability by selective capture using surface-bound siderophores, *Adv. Biol. Chem. 2*, 396-402. DOI: 10.4236/abc.2012.24049

[91] Zheng, T., and Nolan, E. M. (2012) Siderophore-based detection of Fe(III) and microbial pathogens, *Metallomics 4*, 866-880. DOI: 10.1039/C2MT20082A

[92] Pahlow, S., Stöckel, S., Pollok, S., Cialla-May, D., Rösch, P., Weber, K., and Popp, J. (2016) Rapid identification of *Pseudomonas* spp. via raman spectroscopy using pyoverdine as capture probe, *Anal. Chem. 88*, 1570-1577. DOI: 10.1021/acs.analchem.5b02829

[93] Hoegy, F., Celia, H., Mislin, G. L., Vincent, M., Gallay, J., and Schalk, I. J. (2005) Binding of iron-free siderophore, a common feature of siderophore outer membrane transporters of *Escherichia coli* and *Pseudomonas aeruginosa*, *J. Biol. Chem. 280*, 20222-20230. DOI: 10.1074/jbc.M500776200

[94] Schalk, I. J., Kyslik, P., Prome, D., van Dorsselaer, A., Poole, K., Abdallah, M. A., and Pattus, F. (1999) Copurification of the FpvA ferric pyoverdin receptor of *Pseudomonas aeruginosa* with its iron-free ligand: Implications for siderophore-mediated iron transport, *Biochemistry 38*, 9357-9365. DOI: 10.1021/bi990421x

[95] Lebrette, H., Borezee-Durant, E., Martin, L., Richaud, P., Boeri Erba, E., and Cavazza, C. (2015) Novel insights into nickel import in *Staphylococcus aureus*: The positive role of free histidine and structural characterization of a new thiazolidine-type nickel chelator, *Metallomics 7*, 613-621. DOI: 10.1039/c4mt00295d

[96] Ghssein, G., Brutesco, C., Ouerdane, L., Fojcik, C., Izaute, A., Wang, S., Hajjar, C., Lobinski, R., Lemaire, D., Richaud, P., Voulhoux, R., Espaillat, A., Cava, F., Pignol, D., Borezee-Durant, E., and Arnoux, P. (2016) Biosynthesis of a broad-spectrum nicotianamine-like metallophore in *Staphylococcus aureus*, *Science 352*, 1105-1109. DOI: 10.1126/science.aaf1018

[97] Berntsson, R. P., Smits, S. H., Schmitt, L., Slotboom, D. J., and Poolman, B. (2010) A structural classification of substrate-binding proteins, *FEBS Lett. 584*, 2606-2617. DOI: 10.1016/j.febslet.2010.04.043

[98] Bacconi, M., Haag, A. F., Chiarot, E., Donato, P., Bagnoli, F., Delany, I., and Bensi, G. (2017) In vivo analysis of *Staphylococcus aureus* infected mice reveals differential temporal and spatial expression patterns of *fhuD2*, *Infect. Immun.* ASAP, Pub. Date (Web), August 7, DOI: 10.1128/IAI.00270-17. DOI: 10.1128/IAI.00270-17

[99] Podkowa, K. J., Briere, L.-A. K., Heinrichs, D. E., and Shilton, B. H. (2014) Crystal and solution structure analysis of FhuD2 from *Staphylococcus aureus* in multiple unliganded conformations and bound to ferrioxamine-B, *Biochemistry 53*, 2017-2031. DOI: 10.1021/bi401349d

[100] Fukushima, T., Allred, B. E., Sia, A. K., Nichiporuk, R., Andersen, U. N., and Raymond, K. N. (2013) Gram-positive siderophore-shuttle with iron-exchange from Fe-siderophore to apo-siderophore by *Bacillus cereus* YxeB, *Proc. Natl. Acad. Sci. U. S. A. 110*, 13821-13826. DOI: 10.1073/pnas.1304235110
[101] Fukushima, T., Allred, B. E., and Raymond, K. N. (2014) Direct evidence of iron uptake by the Gram-positive siderophore-shuttle mechanism without iron reduction, *ACS Chem. Biol. 9*, 2092-2100. DOI: 10.1021/cb500319n
[102] Lifa, T., Ejje, N., and Codd, R. (2012) Coordinate-bond-dependent solid-phase organic synthesis of biotinylated desferrioxamine B: a new route for metal-specific probes, *Chem. Comm. 48*, 2003-2005. DOI: 10.1039/C2CC17170H
[103] Vértesy, L., Aretz, W., Fehlhaber, H.-W., and Kogler, H. (1995) Salmycin A–D, antibiotika aus *Streptomyces violaceus*, DSM 8286, mit siderophor-aminoglycosid-struktur, *Helv. Chim. Acta 78*, 46-60. DOI: 10.1002/hlca.19950780105
[104] Gwinner, T. (2008) Das Siderophore-Antibiotikum Salmycin, In *Biologie*, Eberhard Karls University of Tubingen, Tubingen, Germany.
[105] Dong, L., Roosenberg, J. M., and Miller, M. J. (2002) Total synthesis of desferrisalmycin B, *J. Am. Chem. Soc. 124*, 15001-15005. DOI: 10.1021/ml300150y
[106] Huber, P., Leuenberger, H., and Keller-Schierlein, W. (1986) Stoffwechselprodukte von mikroorganismen. 233. Mitteilung. Danoxamin, der eisenbindende teil des sideromycin-antibioticums danomycin, *Helv. Chim. Acta 69*, 236-245. DOI: 10.1002/hlca.19860690128
[107] Roosenberg, J. M., 2nd, and Miller, M. J. (2000) Total synthesis of the siderophore danoxamine, *J. Org. Chem. 65*, 4833-4838. DOI: 10.1021/jo000050m
[108] Wencewicz, T. A., Mollmann, U., Long, T. E., and Miller, M. J. (2009) Is drug release necessary for antimicrobial activity of siderophore-drug conjugates? Syntheses and biological studies of the naturally occurring salmycin "Trojan Horse" antibiotics and synthetic desferridanoxamine-antibiotic conjugates, *Biometals 22*, 633-648. DOI: 10.1007/s10534-009-9218-3
[109] Pramanik, A., and Braun, V. (2006) Albomycin uptake via a ferric hydroxamate transport system of *Streptococcus pneumoniae* R6, *J. Bacteriol. 188*, 3878-3886. DOI: 10.1128/JB.00205-06
[110] Bunet, R., Brock, A., Rexer, H. U., and Takano, E. (2006) Identification of genes involved in siderophore transport in *Streptomyces coelicolor* A3(2), *FEMS Microbiol. Lett. 262*, 57-64. DOI: 10.1111/j.1574-6968.2006.00362.x
[111] Patel, P., Song, L., and Challis, G. L. (2010) Distinct extracytoplasmic siderophore binding proteins recognize ferrioxamines and ferricoelichelin in *Streptomyces coelicolor* A3(2), *Biochemistry 49*, 8033-8042. DOI: 10.1021/bi100451k
[112] Vertesy, L., Aretz, W., Fehlhaber, H.-W., and Ganguli, B. N. (1995) Salmycins, a process for their preparation and their use as a pharmaceutical, U. S. Patent, 5,475,094, Dec. 12.
[113] Vertesy, L., Aretz, W., and Fehlhaber, H.-W. (1996) Chelating agents, their preparation from the antibiotics salmycin A,B,C, or D, and their use, U. S. Patent, 5,519,123, May 21.
[114] Yusof, F. (2015) Purification of recombinant protein for industrial use, In: *Recombinant Enzymes - From Basic Science to Commercialization* (Amid, A., Ed.), pp

61-80, Springer International Publishing, Cham. DOI: 10.1007/978-3-319-12397-4 5

[115] Lebendiker, M., and Danieli, T. (2011) Purification of proteins fused to maltose-binding protein, *Methods Mol. Biol. 681*, 281-293. DOI: 10.1007/978-1-60761-913-0 15

[116] Santos, T. M. A., Lammers, M. G., Zhou, M., Sparks, I. L., Rajendran, M., Fang, D., De Jesus, C. L. Y., Carneiro, G. F. R., Cui, Q., and Weibel, D. B. (2018) Small molecule chelators reveal that iron starvation inhibits late stages of bacterial cytokinesis, *ACS Chem. Biol. 13*, 235-246. DOI: 10.1021/acschembio.7b00560

[117] Hsu, S. M., Raine, L., and Fanger, H. (1981) Use of avidin-biotin-peroxidase complex (ABC) in immunoperoxidase techniques: a comparison between ABC and unlabeled antibody (PAP) procedures, *J. Histochem. Cytochem. 29*, 577-580. DOI: 10.1177/29.4.6166661

[118] Mousa, W. K., Athar, B., Merwin, N. J., and Magarvey, N. A. (2017) Antibiotics and specialized metabolites from the human microbiota, *Nat. Prod. Rep. 34*, 1302-1331. DOI: 10.1039/c7np00021a

[119] Wilson, M. R., Zha, L., and Balskus, E. P. (2017) Natural product discovery from the human microbiome, *J. Biol. Chem. 292*, 8546-8552. DOI: 10.1074/jbc.R116.762906

[120] Donia, M. S., and Fischbach, M. A. (2015) Human microbiota. Small molecules from the human microbiota, *Science 349*, 1254766. DOI: 10.1126/science.1254766

[121] Cohen, L. J., Esterhazy, D., Kim, S. H., Lemetre, C., Aguilar, R. R., Gordon, E. A., Pickard, A. J., Cross, J. R., Emiliano, A. B., Han, S. M., Chu, J., Vila-Farres, X., Kaplitt, J., Rogoz, A., Calle, P. Y., Hunter, C., Bitok, J. K., and Brady, S. F. (2017) Commensal bacteria make GPCR ligands that mimic human signalling molecules, *Nature 549*, 48-53. DOI: 10.1038/nature23874

[122] Deriu, E., Liu, J. Z., Pezeshki, M., Edwards, R. A., Ochoa, R. J., Contreras, H., Libby, S. J., Fang, F. C., and Raffatellu, M. (2013) Probiotic bacteria reduce salmonella typhimurium intestinal colonization by competing for iron, *Cell Host Microbe 14*, 26-37. DOI: 10.1016/j.chom.2013.06.007

[123] Konishi, H., Fujiya, M., Tanaka, H., Ueno, N., Moriichi, K., Sasajima, J., Ikuta, K., Akutsu, H., Tanabe, H., and Kohgo, Y. (2016) Probiotic-derived ferrichrome inhibits colon cancer progression via JNK-mediated apoptosis, *Nat. Comm. 7*, 12365. DOI: 10.1038/ncomms12365

[124] Ohlemacher, S. I., Giblin, D. E., d'Avignon, D. A., Stapleton, A. E., Trautner, B. W., and Henderson, J. P. (2017) Enterobacteria secrete an inhibitor of Pseudomonas virulence during clinical bacteriuria, *J. Clin. Investig. 127*, 4018-4030. DOI: 10.1172/JCI92464

Figures and Figure Legends

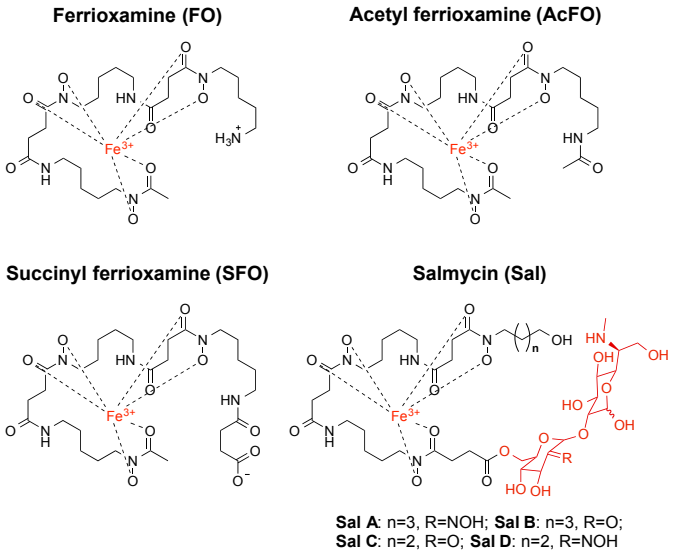

Figure 1. Structures of ferrioxamine siderophores and sideromycins used in this study.

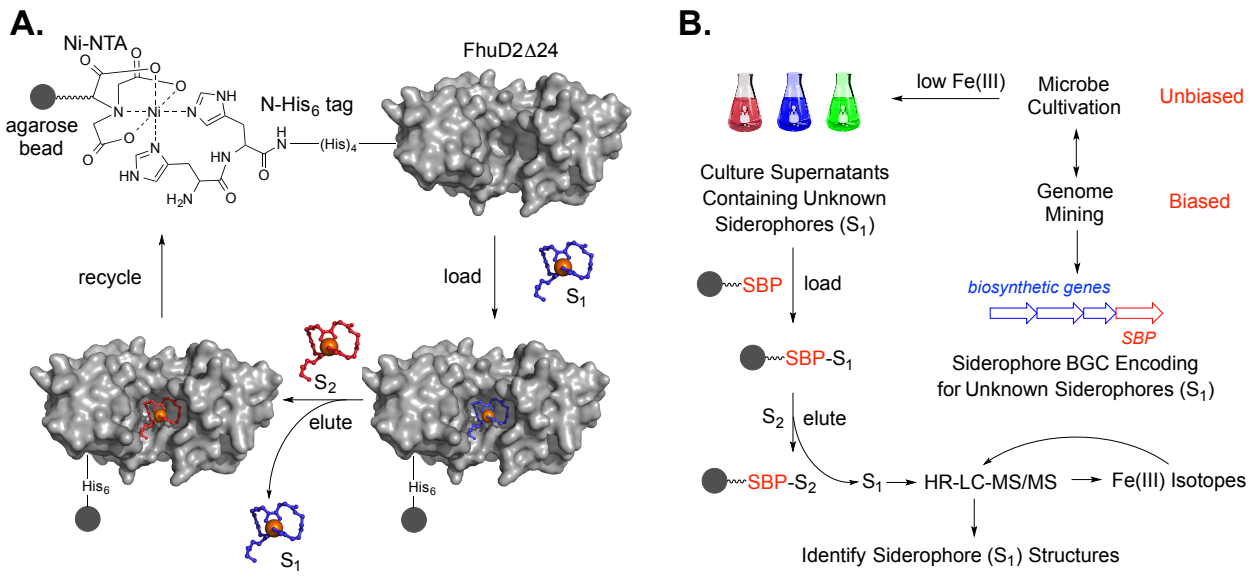

Figure 2. (**A**) General strategy for receptor-mediated purification of bacterial siderophores using SBP resin. An *N*-His_6 tagged siderophore-binding protein (FhuD2 from *S. aureus*) is adhered to a Ni-NTA agarose resin to form the SBP resin. The siderophore of interest (S_1) is loaded to the SBP resin and is bound by FhuD2. A sacrificial siderophore (S_2) is then added to displace siderophore S_1 from the SBP resin. FhuD2 is selective for binding trihydroxamate siderophores. (**B**) Unbiased and biased affinity selection-mass spectrometry (ASMS) strategies for integrating SBP-resins into siderophore natural product discovery platforms.

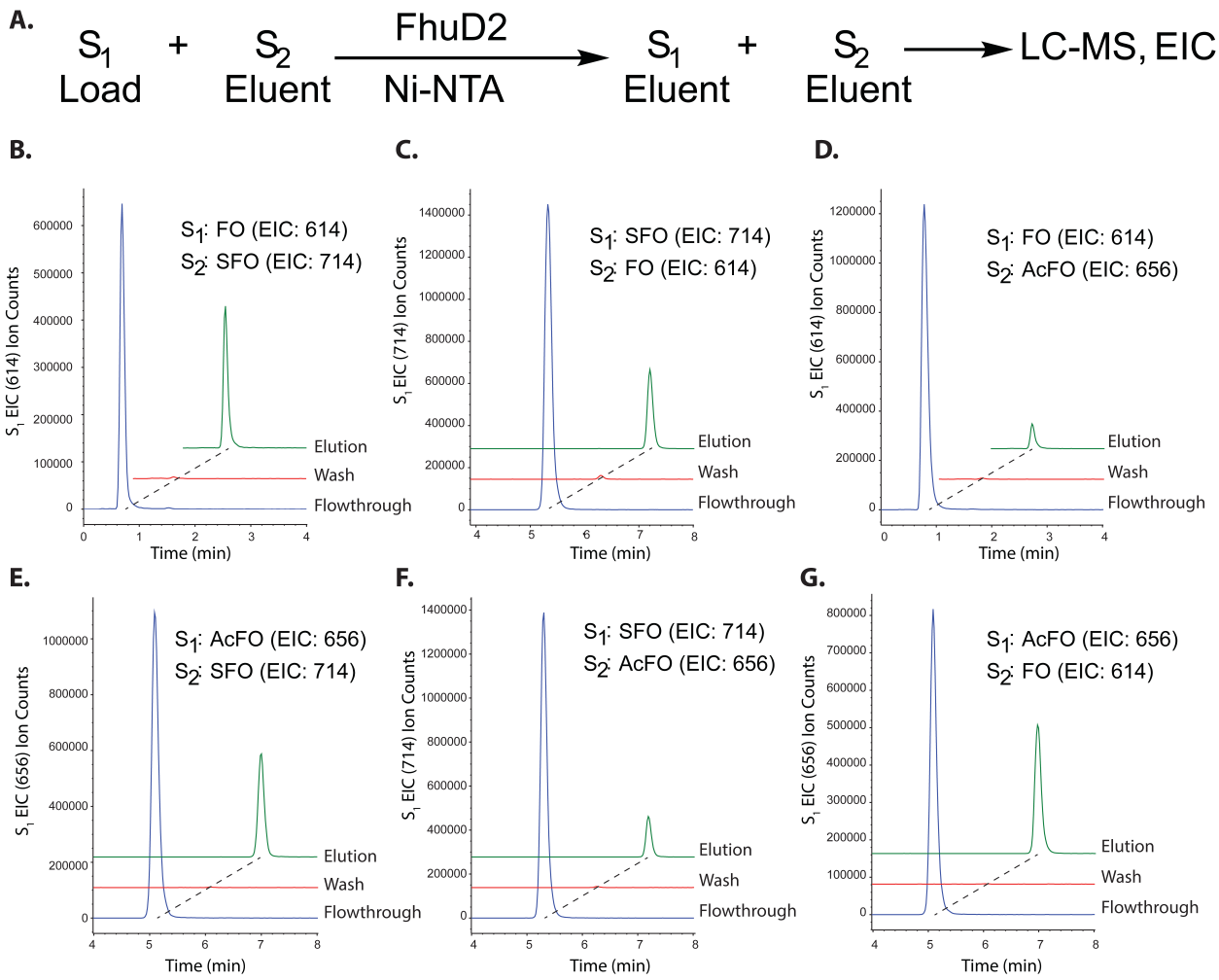

Figure 3. Loading and displacing of siderophores on FhuD2 SBP resin. (**A**) Siderophore S_1 was loaded to the FhuD2 resin and then eluted with siderophore S_2. (**B–G**) All possible combinations of **FO**, **SFO**, and **AcFO** as the loading siderophore (S_1) and eluting siderophore (S_2) were successful in providing S_1 in the final elution from the SBP resin. EIC traces are off-set by 1 minute on the x-axis and a 10% off-set is used on the y-axis. EIC traces are representative of experiments performed in duplicated as independent trials.

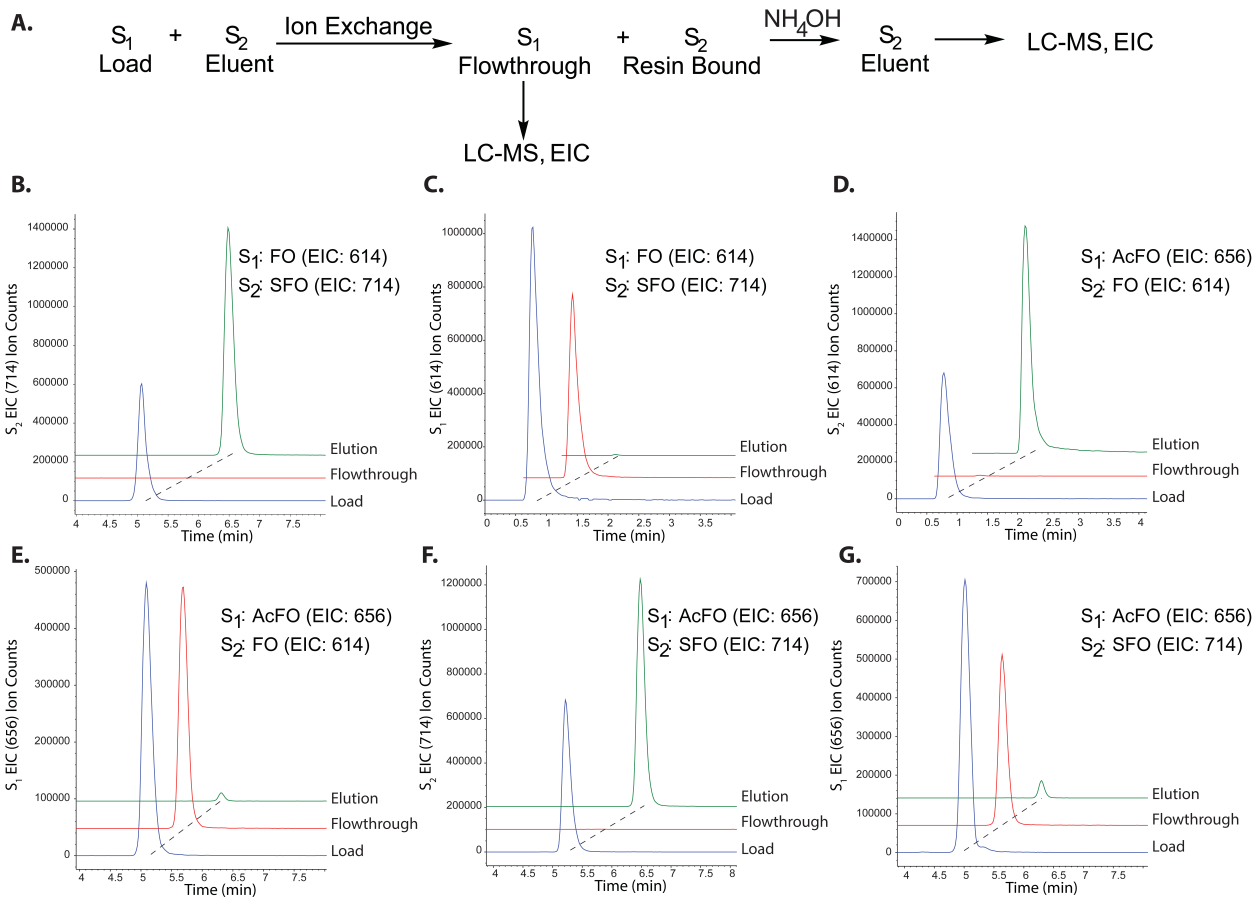

Figure 4. Separation of the siderophore of interest (S_1) and the sacrificial siderophore (S_2) based on net charge using ion exchange chromatography. (**A**) Siderophores S_1 and S_2 were loaded to the ion exchange column. Siderophore S_1 washed through the column and siderophore S_2 was retained on the column and subsequently eluted. (**B**–**G**) All possible combinations of charge positive (**FO**), charge negative (**SFO**), and charge neutral (**AcFO**) were successfully separated as S_1 and S_2. EIC traces are off-set by 0.5 minute on the x-axis and a 10% off-set is used on the y-axis. EIC traces are representative of experiments performed in duplicated as independent trials.

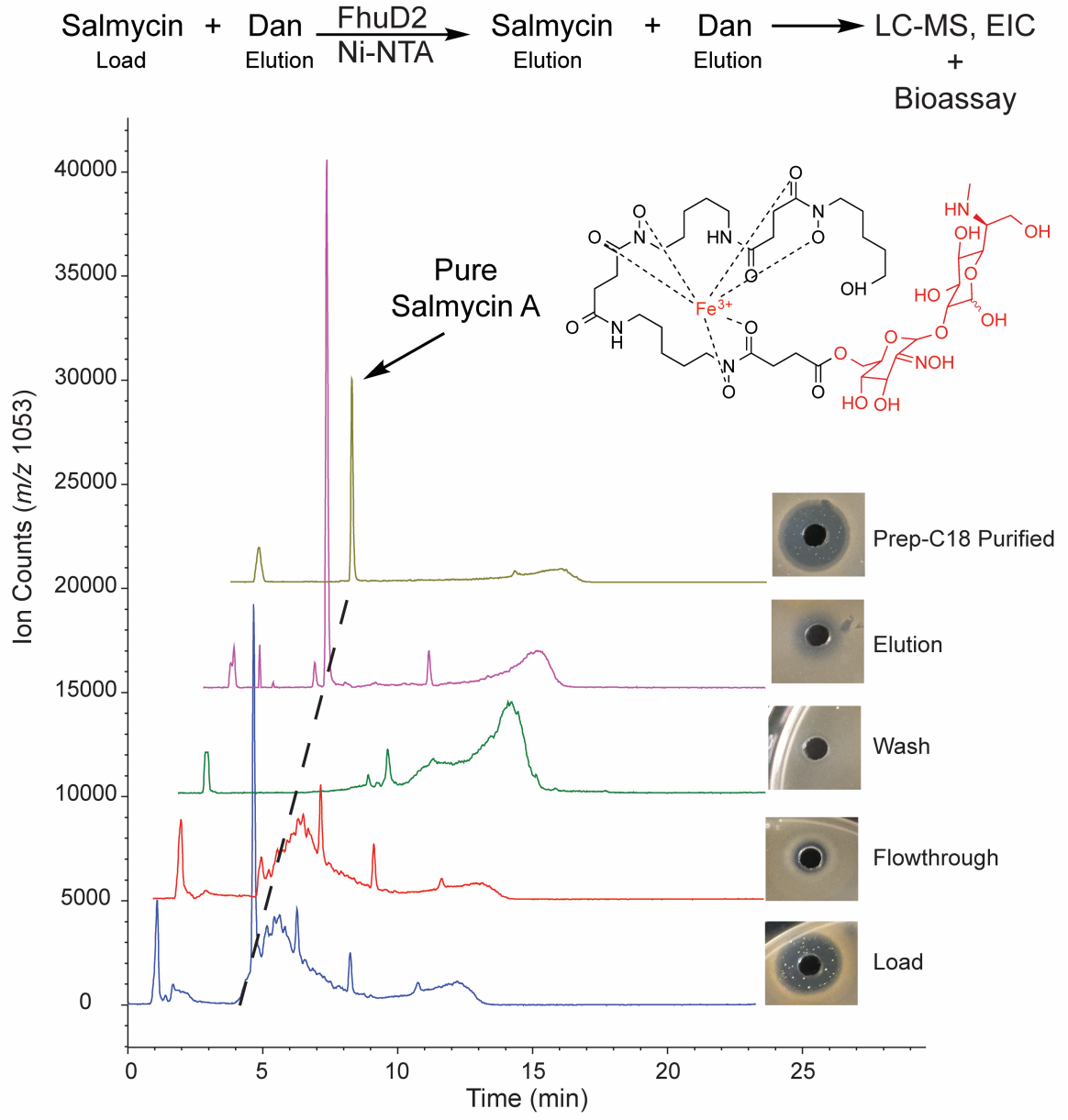

Figure 5. Isolation of pure salmycins from *S. violaceus* DSM8286 culture supernatant by treatment with FhuD2 SBP-resin using danoxamine (**Dan**) as the eluting siderophore. Ion counts for the **Sal A** $[M+H]^+$ ion (*m/z* 1053) were tracked via LC-MS in the column load, flowthrough, wash, elution, and preparative HPLC fractions (Prep-C18 purified) along with growth inhibitory activity in an antibacterial agar diffusion assay using *S. aureus* ATCC 11632. EIC traces are off-set by 1 minute on the x-axis and a 10% off-set is used on the y-axis. EIC traces are representative of experiments performed in duplicated as independent trials.

Graphical Abstract/TOC Figure